



PON Ricerca e
2014- 2020 **Innovazione**



Ministero dell'Istruzione, dell'Università e della Ricerca

**DOTTORATO DI RICERCA IN INGEGNERIA DEI PRODOTTI
E DEI PROCESSI INDUSTRIALI**

UNIVERSITÀ DEGLI STUDI DI NAPOLI FEDERICO II



**DIPARTIMENTO DI INGEGNERIA CHIMICA, DEI MATERIALI E
DELLA PRODUZIONE INDUSTRIALE**

Scuola Politecnica e delle Scienze di Base

**XXX PHD PROGRAMME IN
INDUSTRIAL PRODUCTS AND PROCESSES ENGINEERING**

**Advanced 3D Ultrasonic Non-destructive Evaluation Technique
for CFRP aeronautical applications**

PHD PROJECT SUPERVISOR

Prof. Roberto Teti

PHD PROGRAM COORDINATOR

Prof. Giuseppe Mensitieri

PHD CANDIDATE

Ing. Alberto Bottillo



FRAUNHOFER JOINT LABORATORY OF EXCELLENCE ON
ADVANCED PRODUCTION TECHNOLOGY AT DICMAPI FEDERICO II

Index

ACKNOWLEDGMENTS	i
LIST OF FIGURES	ii
LIST OF TABLES.....	v
Summary.....	1
1. Introduction	3
2. Ultrasonic non-destructive evaluation	5
2.1 Introduction.....	5
2.2 Ultrasounds theory	5
2.3 Ultrasonic non-destructive evaluation (UT NDE)	12
2.3.1 Scanning techniques	14
2.3.2 Transducers.....	17
2.3.3 Ultrasounds representations.....	21
2.3.3.1 A-Scan	22
2.3.3.2 B-Scan	23
2.3.3.3 C-Scan	24
2.3.3.4 D-Scan	25
2.3.3.4 FV-Scan.....	25
3. Advanced UT NDE scanning system	26
3.1 Introduction.....	26
3.2 Scanning system hardware components	26
3.2.1 UT oscillator/detector	28
3.2.2 Digital oscilloscope	28
3.2.3 UT transducer	29
3.2.4 Mechanical UT probe displacement system.....	30

3.2.5 Personal computer	31
3.3 UT FV scanning procedure based on pulse-echo immersion testing.....	32
3.4 UT signal acquisition and processing software	34
3.4.1 Custom-made software – Robotest©.....	34
3.4.2 Ecus Inspection© – UT images generation	37
4 UT NDE case studies.....	42
4.1 Introduction.....	42
4.2 Case Study n° 1 – Metrology characterization and quality assessment of CFRP non-crimp fabric laminates.....	43
4.2.1 CFRP material	43
4.2.2 Impact testing	44
4.2.3 UT FV scanning based on pulse-echo immersion testing of CFRP NCF laminates	46
4.2.4 Metrological characterization of the CFRP NCF laminate	46
4.2.4.1 Correct stacking sequence evaluation	47
4.2.4.2 Thickness calculation	50
4.2.5 Quality assessment of the CFRP NCF laminates	52
4.2.5.1 Damage transition in the stacking sequence.....	52
4.2.5.2 Damage position in the thickness direction.....	54
4.3 Case Study n° 2 - Quality assessment of the adhesive bonding process for CFRP laminates	56
4.3.1 CFRP adhesive bonded joint laminates material.....	56
4.3.2 Adhesive bonding process defects.....	58
4.3.3 UT FV scanning based on pulse-echo immersion testing of CFRP adhesive bonded joint laminates	58
4.3.4 UT images generation of the CFRP adhesive bonded joint laminates	59
4.3.5 Matlab® custom-made analysis software.....	61
4.3.5.1 UT waveforms extracting and saving.....	61
4.3.5.2 Relevant echoes identification.....	62

4.3.5.3 Thickness calculation	63
4.3.5.4 3D thickness reconstruction for the quality assessment of the bonding process...	64
4.4 Case Study n° 3 - Quality assessment of the drilling process for CFRP laminates	69
4.4.1 CRFP drilled laminates material	69
4.4.2 Drilling process defects	70
4.4.3 UT FV scanning based on pulse-echo immersion testing of CFRP Drilled laminates 71	
4.4.4 UT images generation of CFRP Drilled laminates.....	72
4.4.5 Matlab® custom-made Analysis Software.....	73
4.4.5.1 UT waveforms extracting and saving.....	73
4.4.5.2 Relevant echoes identification.....	74
4.4.5.3 Thickness calculation	74
4.4.5.4 3D Thickness reconstruction for the Quality Assessment of the drilling process.	75
4.5 Conclusions.....	77
4.6 Future step.....	78
References	79

ACKNOWLEDGMENTS

I would like to thank Prof. Roberto Teti, for his scientific and human support concerning all the activities I have done during the three years of my PhD. The Fraunhofer Joint Laboratory of Excellence on Advanced Production Technology (Fh-J_LEAPT UniNaples) at the Department of Chemical, Materials and Industrial Production Engineering, University of Naples Federico II, is also gratefully acknowledged for its support to my researches. I would specially like to Tiziana Segreto for her precious helping me in the realization of this thesis work. Moreover, the research activities described in the third case study have been developed in the context of the national MIUR PON Project on “Development of eco-compatible materials and technologies for robotised drilling and assembly processes – STEP FAR” (2014-2017). Finally, I would like to thanks also my whole team work for its constant moral Backing especially in the moments of difficulty and with which I’ve spent the most beautiful memories.

LIST OF FIGURES

Figure 1. Scheme of longitudinal ultrasonic waveforms. The waveform-length, λ , is the distance corresponding to one complete cycle.	7
Figure 2. Transverse waveforms scheme.	7
Figure 3. Diagram of surface (Rayleigh) waveforms propagating at the surface of a metal along a metal/air interface.	8
Figure 4. Diagram of the basic patterns of symmetrical (dilatational) and asymmetrical (bending) Lamb waveforms.	9
Figure 5. Energy absorption vs. distance.	10
Figure 6. Relationship (by vectors) of all possible reflected and refracted waveforms to an incident longitudinal waveform.	12
Figure 7. Ultrasonic complete waveform of a work piece defect-free.	16
Figure 8. Ultrasonic complete waveform of a work piece containing a defect which correspond the Defect echo.	17
Figure 9. Piezoelectric crystal behaviour under voltage stress.	18
Figure 10. (a) Straight beam transducer and (b) its scheme.	19
Figure 11. (a) Angle beam transducer and (b) its scheme.	19
Figure 12. Damped response of a pulsed stimulate transducer.	19
Figure 13. Section of a double transducer probe.	20
Figure 14. Non-focused UT ultrasonic beam.	21
Figure 15. Focused UT probe scheme.	21
Figure 16. A-scan signal-inspection scheme.	22
Figure 17. B-scan representation.	23
Figure 18. C-scan presentation (coloured circles are presenting areas of discontinuity).	24
Figure 19. D-Scan representation.	25
Figure 20. Utilized UT NDE system components/scheme.	27
Figure 21. Krautkrämer USIP 12.	28
Figure 22. Digital oscilloscope LeCroy 9400.	29
Figure 23. Focused high frequency probe.	29
Figure 24. RX60L work volume.	31
Figure 25. UT FV scanning procedure based on pulse-echo immersion testing (a) execution and (b) its scheme.	33
Figure 26 Software Robotest© main menu.	35
Figure 27. Full Volume Scan user interface.	36
Figure 28. Set-up RX60L user interface.	37
Figure 29. First Ecus Inspection© user interface.	38
Figure 30. “Change Limits” user interface: selected UT waveform and its sub-gates.	39
Figure 31. Example of a complete UT waveform with three sub-gates and relative UT images.	40
Figure 32. 16 UT images of an impacted CFRP laminate. Each image corresponds to 1/16 TH of the laminate thickness.	41
Figure 33. (a) Not-impacted “QHL3IM1” laminate and (b) impacted “QHL3IM2” laminate.	44
Figure 34. CEAST Fractovis MK4 falling weight machine.	44
Figure 35. Cylindrical indenter with hemispherical nose.	45
Figure 36. Appropriate fixture to clamp the rectangular specimens.	45
Figure 37. (a) UT FV scanning of the CFRP NCF laminate; (b) scanned area 11 x 15 mm.	46

Figure 38. First Ecus Inspection© user interface with the 2D scheme of the scanned area of the QHL3IM1 laminate and the UT waveform relative to the scan point selected through the red cursor.	47
Figure 39. “Change Limits” user interface showing the selected complete UT waveform and its 16 time sub-gates (in the red rectangle).	48
Figure 40. Sixteen UT images of the not impacted quadriaxial laminate QHL3IM1. Each UT image, arranged in succession from left to right and from top to bottom, relates to 1/16 th of the laminate nominal thickness comprising two diverse consecutive fiber orientations in the stacking sequence [+45°/0°/-45°/90°, +45°/0°/-45°/90°, 90°/-45°/0°/+45°, 90°/-45°/0°/+45°]s.	49
Figure 41. Time gate set on the Frontal and Back echoes of the QHL3IM1 laminate UT waveform.	50
Figure 42. Time gate divided into 4 time sub-gates.	52
Figure 43. 4 UT images for low energy (9 J) impacted NCF laminate specimen QHL3IM2: (a) surface damage, (b) and (c) internal damage, (d) in-plane projection of the total damage.	53
Figure 44. 4 UT images for medium energy (20 J) impacted NCF laminate specimen QHL3IM5: (a) surface damage, (b) and (c) internal damage, (d) in-plane projection of the total damage.	53
Figure 45. Four UT images for high energy (40 J) impacted NCF laminate specimen QHL3IM8: (a) surface damage, (b) and (c) internal damage, (d) in-plane projection of the total damage.	53
Figure 46. 16 UT images of the QHL3IM impacted laminate.	54
Figure 47. CFRP adhesive bonded joint: (a) Frontal and (b) side view.	57
Figure 48. Form and dimension of Test Specimen [37].	57
Figure 49. Different failure ways of the adhesive bonding joint.	58
Figure 50. UT FV scan of the adhesive bonded joint laminate with the two scan directions x-y.	59
Figure 51. Adhesive bonding joint laminate scanned area of 15 x 15 mm (red square).	59
Figure 52. Typical UT waveform of the UT volumetric file for the CFRP adhesive bonded joint with the time gate divided in 16 time sub-gates.	60
Figure 53. Sixteen UT images of the adhesive bonded joint laminate. Each UT image, arranged from left to right and from top to bottom, relates to 1/16 of the laminate nominal thickness.	60
Figure 54. Firsts code line of the custom-made Matlab® software developed at the Fraunhofer Joint Laboratory of Excellence on Advanced Production Technology [39].	61
Figure 55. (a) Generic UT waveform of the CFRP adhesive bonded joint laminates with the two couples of relevant echoes: the 1 st composed by the Frontal and the Back echoes, the 2 nd one by the middle echoes; (b) laminate side view with the interfaces corresponding to the relevant echoes.	63
Figure 56. Generic UT waveform of the CFRP adhesive bonded joint laminates with the correspondence to the thickness portions they represent.	64
Figure 57. Adhesive thicknesses measured (a) along the x direction at y = 0, 3, 6, 9, 12, 15 mm and similarly (b) along the y direction at x = 0 mm, x = 0, 3, 6, 9, 12, 15 mm).	65
Figure 58. Interpolated curves of the adhesive thicknesses measured along (a) the x and (b) y direction of scan.	66
Figure 59. Adhesive (a) top (yellow) and bottom (blue) surfaces and (b) their fitting.	67
Figure 60. Colour map of the total thickness variation of the entire CFRP sample (two external laminates plus adhesive layer): (a) 3D view, (b) top view.	68
Figure 61. CFRP drilled laminate.	69
Figure 62. CFRP laminates mechanical joints through screws and bolts.	70
Figure 63. (a) Peel-up and (b) push-out delamination.	71
Figure 64. Pulse-echo UT FV immersion scanning on the CFRP drilled laminates with the two scan directions x-y.	71
Figure 65. CFRP Drilled laminates with the scanning area of 14 x 14 mm (red square).	72

Figure 66. Sixteen UT images of the CFRP drilled laminate. Each UT image, arranged from left to right and from top to bottom, relates to 1/16 of the laminate nominal thickness.	73
Figure 67. Generic UT waveform of the CFRP drilled laminate with one couple of relevant echoes: the Frontal and the Back echoes.	74
Figure 68. Generic UT waveform of the CFRP drilled laminate with the indication of the total laminate thickness and of the adhesive layer thickness.	75
Figure 69. Cubic interpolation of the total CFRP drilled laminate thickness. The presence of Volcano effect is clearly evident.	76
Figure 70. View from above of the total CFRP drilled laminate thickness showing the Volcano effect orientation at -45° and a thickness variation ranging between 4.78 and 5.52 mm.	76

LIST OF TABLES

Table 1. PC characteristics.....	32
Table 2. Parameters of the impact testing plan	45
Table 3. Thicknesses of each NCF composite portions comprising of two diverse consecutive fiber orientations in the laminate stacking sequence.	51
Table 4. Damage position direction, delamination position and maximum delamination area extension position in the thickness direction for each impacted sample.....	55

Summary

In this thesis work, an advanced ultrasonic (UT) non-destructive evaluation (NDE) system [1, 2, 3] using a robotic arm for probe displacement and a custom-made software code (developed in LabView© environment) was utilized to perform a reliable and repeatable UT Full Volume (FV) scanning based on pulse-echo immersion testing on three different carbon fiber reinforced plastic (CFRP) aeronautical components.

In particular, the first chapter is an introduction to UT NDE techniques and of the CFRP materials, starting from their first appearance in the industrial field.

The second chapter focuses on the ultrasonic NDE methods. In particular after a general definition of the NDE, the key concepts of the ultrasounds theory are illustrated. Finally, the NDE based on the ultrasounds are explained in detail describing, clarifying the physical principles, the different scanning techniques, the kind of UT probes and the main ultrasounds representations.

The third chapter regards the description of the UT NDE scanning system utilized to perform the UT inspections: first the hardware components are listed with the relative features, then the scanning procedure and the custom-made software functionalities are explicated.

The fourth and last chapter is the most important as it concerns the application of an advanced UT NDE system (described in the previous chapters) on three cases study regarding three different industrial applications of CFRP materials both in terms of fabrication methods and applied technologies and in terms of the UT inspection goals.

In fact, the first case study is focused on the UT inspection of CFRP non-crimp fabric (NCF) laminates allowing two different UT analysis:

- 1) metrological characterization of a CFRP NCF not impacted laminate, in terms of:
 - a. correct stacking sequence evaluation
 - b. laminate thickness calculation
- 2) quality assessment of 7 CFRP NCF impacted laminates (with different impact energies) in terms of:
 - c. analysis of damages transition in the stacking sequence
 - d. calculation of the damages position in the laminates thickness direction

The second case regards the quality assessment of the bonding process of CFRP adhesive bonded joint laminates in terms of:

- adhesive layer homogeneity evaluation
- 3D thickness reconstruction (both adhesive layer and entire laminates)

The third case study concerns the quality assessment of the drilling process of CFRP drilled laminates [4] in terms of:

- drilling process evaluation
- push-out delamination characterization through a 3D thickness reconstruction

In particular, the analysis discussed in the second and third case study are carried out through a second custom-made software properly developed in Matlab® environment that provides a 3D thickness reconstruction of the defects [5] by processing the UT volumetric scanning data. Finally, are reported the proper conclusions and the future steps

1. Introduction

The era of modern ultrasonic techniques started about 1917 with Langevin's use of high-frequency acoustic waves and quartz resonators for submarine detection [6]. Underwater detection systems were developed for submarines navigation in World War I and in particular after the tragic sinking of the Titanic in 1912 for the detection of underwater icebergs.

In 1928, the Soviet scientist Sergei Y. Sokolov proposed a through-transmission technique for flaw detection in metals [7] In this technique, he showed that flaws in metals could be detected by monitoring ultrasonic energy transmitted across the metal itself. However, the resolution of his experimental device was poor but the Sokolov's technique remains the basis of the modern ultrasonic non destructive testing techniques [8].

The first flaw detecting device and measuring instrument was patented by Floyd Firestone [9] but the turning point was given by the introduction of piezoelectric crystal transducers by James F. McNulty for ultrasonic testing [10].

Since that time, the field of ultrasonic (UT) non-destructive evaluation (NDE) has grown enormously, with applications found in science, industry, medicine and other areas.

In modern manufacturing, UT NDE methods are utilized for the detection of surface, subsurface and internal flaws (e.g. cracks, laminations, cavities, pores, inclusions, bonds, etc.) in different types of materials (e.g. metals, composite materials, plastics) [11-13].

In aeronautical field, the UT NDE technique is are largely used for materials inspection and part quality control. Using UT NDE testing, defective parts can be identified and removed before they are put into service. Moreover, UT testing permits to examine aircraft structures without disassembling them.

Nowadays, the employment of composite materials such as carbon fiber reinforced plastic (CFRP) is steadily grown for the construction of light-weight airplanes. The CFRP composites are successfully utilized for their high strength-to-weight ratio, high stiffness-to-weight ratio and rigidity properties [14, 15] for the outer and central wing-box, fuselage, wings, tail, empennage, etc. [16, 17]. The two leader aeronautical companies (Airbus and Boeing) utilize CFRP composites for their airplane construction in order to achieve a reduction of the aircraft weight and consequently a fuel consumption decrease [18-20]. The first generation commercial aircrafts made of a large number of CFRP composite parts were

the Boeing 787 Dreamliner (50% composites components) and the Airbus A350 XWB (52% composites components) [1, 21].

Despite these advantages, the main drawback of the CFRP composite utilization is that damages can occur, at several scales, within this composite material (e.g. damage in the matrix and/or fiber or delamination) without an external indication [5, 22]. Consequently, each produced composite structure needs to be inspected in order to evaluate the presence of possible defects [4, 23] and to prevent a catastrophic failure of the airplane [24].

2. Ultrasonic non-destructive evaluation

In this chapter, after a concise exposure about the non-destructive evaluation (NDE) and the ultrasounds theory, the ultrasonic NDE technique will explained in detail.

2.1 Introduction

The term non-destructive evaluation (NDE) implies testing, inspection and examination performed to identify, localize and measure possible defects, discontinuities or non-conformities to the material specifications, without damage or degradation of the product under examination [25, 26]. The presence of a defect can reduce the mechanical properties of the product or determine its disposal. There are several NDE techniques depending on the physical principle on which they are based (e.g. visual inspection, acoustic emission, ultrasounds, X-ray, eddy current, penetrant liquid or thermal analysis). Each technique could be suitable to characterize same type of defects and at the same time they could not for other types. Analogously they could be performed on certain materials and not on others. For these reasons, it is very important to choose the more appropriate NDE technique in order to obtain the best result of the inspection. In this research work an ultrasonic non-destructive evaluation (UT NDE) technique was used in order to perform an UT full volume scanning based on pulse-echo immersion testing on diverse aeronautical components.

2.2 Ultrasounds theory

UT waveforms are high frequency mechanical vibrations (> 20 KHz) consisting in oscillations of atomic or molecular particles of a substance around their equilibrium positions. When the atomic or molecular particles of an elastic material is displaced from their equilibrium positions by any applied force, internal stress acts to restore the particles to their original positions. Due to the interatomic forces between adjacent particles of material, a displacement at one point induces displacements at neighbouring points and so on, thus propagating a stress-strain waveform. UT waveforms are also similar to a light waveforms because both obey a general waves equation and travel in a given homogeneous medium at a

characteristic velocity and attenuation of energy that depends on the medium properties. As well as light beams, the UT waveforms are:

- reflected when they bump into a surface
- refracted when they cross a boundary between two substances with different characteristic velocities
- diffracted at edges or around obstacles and scattering by rough surfaces reducing the intensity of the beam

Therefore, the behaviour of the UT waveforms is essentially the same of the sound one, in fact they can propagate in any elastic medium which can be solid, liquid, or gaseous (not in vacuum). The particles of the elastic medium move, but they do not migrate from their initial spatial orbits; only the energy travels through the medium. The amplitude of UT waveforms depends on the amount of energy supplied. The relation between velocity, frequency and waveform-length is given by:

$$v = f \cdot \lambda$$

where v is velocity (in meters/second), f is frequency (in hertz), and λ is waveform-length (in meters/cycle).

On the basis of the particle displacement mode, ultrasonic waveforms are classified as:

- Longitudinal waveforms,
- Transverse waveforms,
- Surface waveforms (Rayleigh),
- Lamb waveforms.

Longitudinal waveforms (or compression waveforms) are the type of UT waveforms most widely used in the UT NDE. They travel into the materials as a series of alternate compressions and rarefactions in which the particles transmitting the waveform vibrate Back and forth in the waveforms travel direction (Figure 1). The distance between two consecutive crests (corresponding to a complete cycle of rarefaction and compression) is the waveform-length, λ . Longitudinal UT waveforms are readily propagated in liquids and gases as well as in elastic solids. The velocity of UT longitudinal waveforms is about 6000 m/s in steel, 1500 m/s in water and 330 m/s in air.

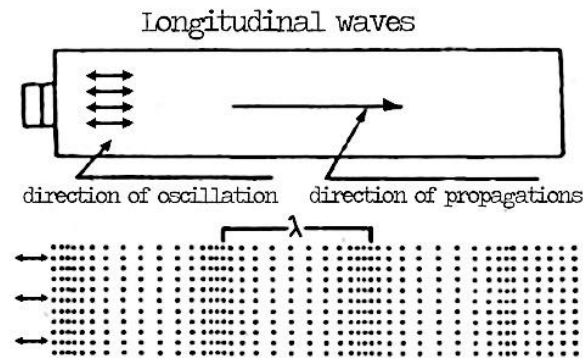


Figure 1. Scheme of longitudinal ultrasonic waveforms. The waveform-length, λ , is the distance corresponding to one complete cycle.

Transverse waveforms are also used in the materials UT inspection and they are commonly visualized in terms of vibrations of rope that is shaken rhythmically, in which each particle vibrates up and down in a perpendicular plane to the direction of propagation. A transverse waveform is illustrated schematically in Figure 2. Unlike what happens to the longitudinal waveforms, the transverse waveforms to propagate need each particle exhibits a strong force of attraction to its neighbours so that as a particle moves Back and forth it pulls its neighbour with it, thus causes that their velocity is about 50% of the longitudinal one for the same material. Moreover, air and liquid not particularly viscous (e.g. water) will not support transverse waveforms propagation.

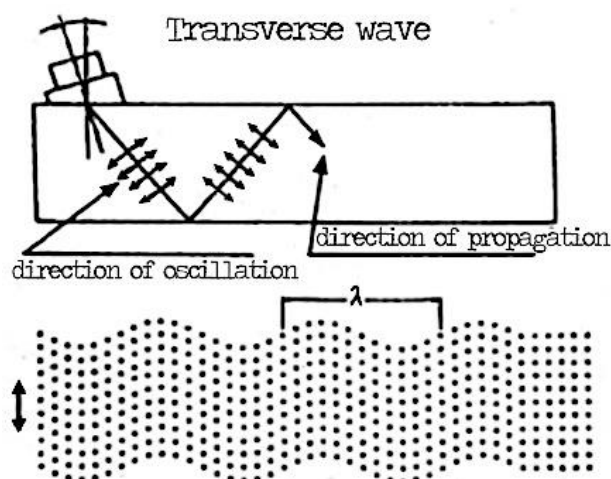


Figure 2. Transverse waveforms scheme.

Surface waveforms (also named Rayleigh waveforms) are another type of UT waveform used in the inspection of flat or curved surfaces of relatively thick solid parts. In fact, for the propagation of the surface waveforms they must travel along an interface bounded on one side by the strong elastic forces of a solid and, on the other side, by the practically negligible elastic forces between gas molecules. Surface waveforms are subject to attenuation in a given material as for the longitudinal and transverse ones. They have a velocity approximately 90% of the transverse waveform one in the same material. The region within which these waveforms propagate with effective energy is not much thicker than about one waveform-length beneath the surface of the metal. At this depth, waveform energy is about 4% of that at the surface, and the amplitude of oscillation decreases sharply to a negligible value at greater depths. Surface waveforms follow contoured surfaces for this reason they can be used to inspect parts with complex contours. In surface waveforms, particle oscillation generally follows an elliptical orbit, as shown schematically in Figure 3.

Lamb waveforms, also known as plate waveforms because they propagate in plates (made of composites or metals) only a few waveform-lengths thick. A Lamb waveform consists of a complex vibration that occurs throughout the thickness of the material. The propagation characteristics of Lamb waveforms depend on the density, elastic properties, and structure of the material as well as the thickness of the specimen and the frequency.

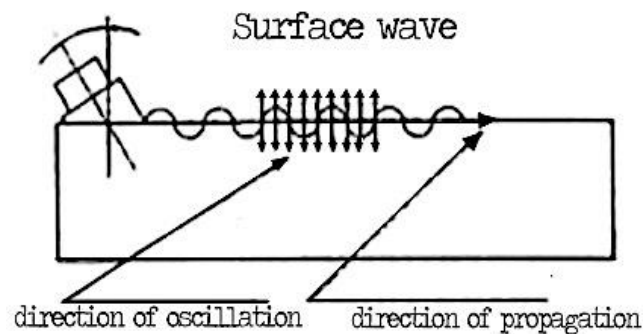


Figure 3. Diagram of surface (Rayleigh) waveforms propagating at the surface of a metal along a metal/air interface.

There are two basic forms of Lamb waveforms (Figure 4):

- Symmetrical, or dilatational
- Asymmetrical, or bending

The form is determined by whether the particle motion is symmetrical or asymmetrical with respect to the neutral axis of the sample. Each form is further subdivided into several modes having different velocities, which can be controlled by the angle at which the waveforms enter the sample. In symmetrical (dilatational) Lamb waveforms, there is a compression (longitudinal) particle displacement along the neutral axis of the plate and an elliptical particle displacement on each surface while in the asymmetrical (bending) ones, there is a shear (transverse) particle displacement along the neutral axis of the plate and an elliptical particle displacement on each surface. As happens for other types of waveforms, independently from the atomic vibration trajectories, when the UT waveforms travel within an elastic material there is an energy attenuation phenomena.

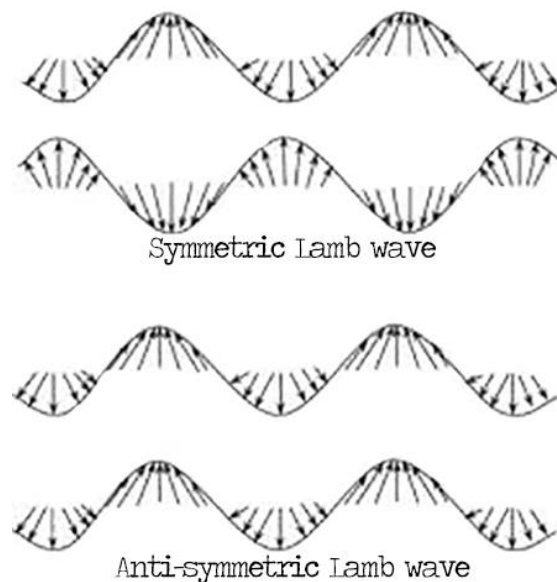


Figure 4. Diagram of the basic patterns of symmetrical (dilatational) and asymmetrical (bending) Lamb waveforms.

In fact exist energy distortion phenomena from the main beam such as reflection, refraction, diffraction and scattering, and absorption phenomena. As their consequence and due to the material opposite to the waveforms propagation mechanical energy converts heat. Thus, for each material, it is recognized the existence of an absorption coefficient, whose magnitude depends not only on the medium but also on the waveform frequency, is in particular it is directly proportional to the frequency square and inversely proportional to the density and to the cube of the waveforms propagation velocity (Figure 5).

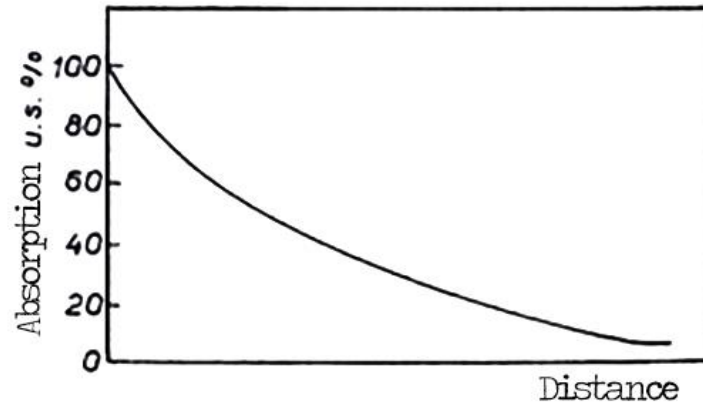


Figure 5. Energy absorption vs. distance.

Following is reported the analytical formula that defines the UT waveform intensity attenuation during its travel within the material:

$$I(x) = I(0) \cdot e^{-Kx}$$

where $I(x)$ is the beam intensity after it has traveled for a x distance, $I(0)$ is the initial intensity and K is the absorption coefficient. An other phenomenon connected to the utilized instruments is what happens when a bundle of UT waveforms crosses two different materials; in this case, in fact, at the interface, a part of the beam is reflected and a part is transmitted. The transmitted quantities and reflected are function of the chosen materials through a physical characteristic of each medium defined as acoustic impedance:

$$Z_1 = \frac{\rho}{v_1}$$

This characteristic is used in the UT inspection to select the suitable materials for the effective transfer of acoustic energy between components in the UT inspection systems. If the impedances of the two materials are equal there will be no reflection while if they differ greatly (as between a metal and air, for example), there will be virtually complete reflection. The percentage of incident energy reflected from the interface between two materials depends on the ratio of acoustic impedances (Z_2/Z_1) and the angle of incidence.

When the angle of incidence is 0° , (normal incidence), the reflection coefficient, R , which is the ratio of reflected beam intensity, I_r , to the incidence beam intensity, I_i , is given by:

$$R = \frac{I_r}{I_i} = \left[\frac{(Z_2 - Z_1)}{(Z_1 + Z_2)} \right]^2 = \left[\frac{(r - 1)}{(r + 1)} \right]^2$$

where Z_1 is the acoustic impedance of the medium 1, Z_2 is the acoustic impedance of the medium 2 and r is the impedance ratio and is equals to (Z_2/Z_1) . The transmission coefficient, T , can also be calculated as the ratio of the intensity of the transmitted beam, I_t , to that of the incident beam, I_i , from:

$$T = \frac{I_t}{I_i} = \frac{4Z_2 \cdot Z_1}{(Z_1 + Z_2)^2} = \frac{4r}{(r + 1)^2}$$

Only when an UT waveform is incident at right angles on an interface between two materials (normal incidence; that is, angle of incidence = 0°) do transmission and reflection occur at the interface without any change in beam direction. At any other angle of incidence, the phenomena of mode conversion (a change in the nature of the waveform motion) and refraction (a change in direction of waveform propagation) must be considered. These phenomena may affect the entire beam or only a portion of the beam, and the sum total of the changes that occur at the interface depends on the angle of incidence and the velocity of the ultrasonic waveforms leaving the point of impingement on the interface. The UT waveforms, accidents, reflected and transmitted are in the same plane, and in addition, the incident and the reflected waveform form the same angle with the normal to the separation surface between the two materials. Moreover the longitudinal waveforms give rise to reflex and refractors waveforms with longitudinal and transverse components (Figure 6). This is a consequence of the different propagation speed between the longitudinal and the transverse waveforms. In particular, it occurs that:

$$V_T < V_L \Rightarrow \alpha_T < \alpha_L$$

By increasing the incidence angle is it possible to reach a value that make the longitudinal waveforms completely reflected ($\beta_L = 90^\circ$). This angle is called first critical angle. Increasing

the incidence angle further, it is possible to achieve a value for which even the transverse waveforms stop to be transmitted (second critical angle).

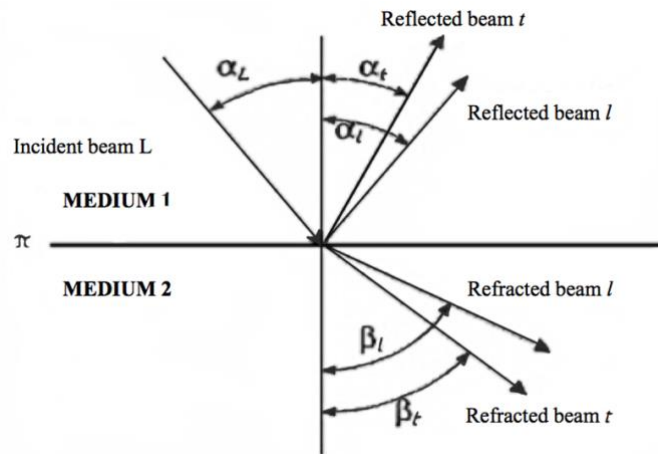


Figure 6. Relationship (by vectors) of all possible reflected and refracted waveforms to an incident longitudinal waveform.

The general law that describes waveform behaviour at an interface is known as Snell's law. Although originally derived for light waveforms, Snell's law applies to acoustic waveforms (including ultrasound) and too many other types of waveforms. According to Snell's law, the ratio of the sine of the angle of incidence to the sine of the angle of reflection or refraction equals the ratio of the corresponding waveform velocities, as reported in the following formula. Snell's law applies even if mode conversion takes place.

$$\frac{\sin \alpha}{\sin \beta} = \frac{V_1}{V_2}$$

2.3 Ultrasonic non-destructive evaluation (UT NDE)

The ultrasonic non-destructive evaluation technique (UT NDE) is a non-destructive control in which beams of high-frequency sound waveforms are introduced into materials for the detection of flaws in the material [27]. The UT waveforms traveling into the material have some loss of energy (attenuation) and are partially or totally reflected at the possible discontinuity interfaces. In this technique the reflected beam is displayed and then analysed to verify the presence of flaws or discontinuities and, if present, their location. The quantity of

reflected energy depends mainly on the physical state of the materials constitute the defect. In particular defects containing gas (e.g. inclusions, pores, cracks, laminations, flakes, etc.) reflect almost completely the UT waveforms while metal/liquid or metal/solid interfaces reflect partially the UT beams [28]. Following are reported the main methods used from the common UT instruments to detect the defects:

- check the presence of echoes reflected by internal defects
- check the time employed by the UT signal to cross the whole specimen [29]
- check the attenuation suffered from the UT waveforms because of the absorption or scattering during it travel into the work piece
- check the spectral response for the transmitted or reflected signal

The first and more common UT NDE employment is to detect and characterize internal defects, to make thickness measurement, to evaluate the extension of corrossions, but also (in less cases) to determine physical properties, structure, grain size, and elastic constants of materials. Most UT NDE systems include the following basic equipment:

- electronic clock
- electronic signal generator or pulser that produces impulses of alternating voltage (in the form of negative spike or square waveform) when electronically triggered
- sending probe that emits the UT waveforms when it is stressed by voltage
- coupling medium to transfer UT signal from the sending probe to the sample and vice-versa
- receiver probe that receive the reflected UT beam converting the mechanical vibration into impulse of alternating voltage
- electronic amplifier to amplify or demodulate the UT signal
- display device (e.g. CRT, digital oscilloscope, etc.) to visualize or eventually record the UT signal
- an electronic clock to control the operation of system components

As pre mentioned, exist probes both transmitter and receiver named transducers. Among the advantages of the UT NDE can be listed:

- high sensitivity of the control, which, in some cases (e.g. utilizing focused probes), allows to detect very small defects, and to determine position, nature, size and orientation
- high power of penetration allowing the detection of internal very deep flaws that is to examine high thicknesses (about 6 meters)
- possibility to inspect from only one surface of the specimen
- low investment costs and minimum of management
- no danger for the operator
- immediate results, allowing its utilization for in-line production inspections (e.g. for quality control in industries)
- portability
- possibility to perform volumetric scanning

On the other hand there are some disadvantages related to the nature and the geometry of the inspected material, difficulty to detect surface defects, to inspect rough specimen, and the need for experienced operators. Finally are required standard references both for calibrating the equipment and for characterizing defects. The major type of the detectable defects, which can be present in the raw material or resulting after a fabrication process are: voids, flakes, inclusions, cracks, pipe, delamination etc. UT NDE can also be used to measure the thickness of metal sections and to assess the loss of thickness from corrosion inside chemical-processing equipment.

2.3.1 Scanning techniques

Exist different UT NDE techniques and their main distinction is into:

1. Transmission Technique (or by transparency).
2. Reflection Technique (or pulse-echo technique).

In the transmission technique two distinct probes for UT signal transmitting and receiving are used. The transmitter probe is positioned on a sample surface while the receiver one is positioned on the opposite surface, which implies that two opposite specimen surfaces must be accessible for the probes positioning. In this scan technique the term pitch-catch is often utilized to indicate the two distinct probes employment. The presence of a defect is verified

by comparing the received UT signal with a reference one obtained from an inspection on a standard sample. If a loss of UT energy is present then it is very probable that a defect is present in the examined sample. Instead, the reflection technique (or pulse-echo) [30] is based on the properties of the UT beam to be reflected whenever it encounters an imperfection or discontinuity in the material in which it propagates, generating echoes generally accompanied by an attenuation of the sound energy. Differently to the transparency technique, only one specimen surface must be accessible. In the pulse-echo technique a generator/detector send electric impulses to the transducer that, thanks to the piezoelectric phenomenon, generates and transmits UT waveforms to the sample under inspection. The reflected part of the UT signal came back to the transducer, where the inverse piezoelectric phenomenon occurs converting the UT signal into mechanical vibrations which are sent to the generator/detector. The received UT vibrations are subject to the last conversion into alternating voltage and finally sent to an oscilloscope to be displayed.

The UT NDE technique can also distinguish between contact and non-contact mode, depending on whether the transducer is directly or indirectly coupled with the sample surface. UT signal transmission is only possible if there is not a layer of air between the probe and the specimen (as the air is a UT vibrations insulator) therefore it is necessary a coupling between them. If this coupling is realised without the utilization of any medium it has the contact mode (or direct mode), vice versa it has the non-contact mode. The coupling medium can be a layer of liquid or pasty material as water (common or emulsified), oil or grease. Independently from the employed mode, when the UT signal encounters the top sample surface and (after traveling) the opposite bottom one its specular reflection occurs generating two echoes in the UT signal (Figure 7). If these surfaces are parallel the reflected UT signal repeats the outward path in the specimen material returning to the probe. The not reflected remaining UT signal part is again reflected towards the bottom specimen surface generating a series of repetitions.



Figure 7. Ultrasonic complete waveform of a work piece defect-free.

In pulse-echo technique any defect is detectable only if the defect is situated on the UT signal trajectory and if it has a little surface perpendicular to the UT beam so that its reflection can occur. This reflection will correspond to another echo in the UT signal (named defect echo) between the Frontal and the Back ones, as well as a Back echo attenuation (Figure 8). The temporal distance between the Frontal and the Back echoes is called time of flight (ToF), and it is the time employed by the UT signal to cross the material thickness twice (to and fro). The reflection technique allows to establish the depth of the defect, through the calculation of the defect echo temporal position and knowing the ultrasounds propagation velocity in the examined material, thus utilizing the simple formula:

$$v = \frac{s}{(dt/2)}$$

where v is the UT velocity in the material and dt is the time of flight, which is divided by 2 because the UT beam cross the specimen material twice. The main difficulty of this type of analysis is that, as previously mentioned, echoes often give multiple repetitions, due to further reflection of the beam. These undesired echoes can easily mislead the operator about the nature of the signal under consideration. Other inconvenient occurs when the defect is wider than the UT beam. In this case the defect reflects almost all its energy, therefore the Back echo will not appear. Finally, a sample with small but numerous defects, spreads the incident beam in all directions, so it is difficult to identify the nature of those discontinuities. Moreover the attenuation of the UT signal can limit the achievable UT distance and consequently the measurable thickness. This limit varies depending on material and on work frequency. As the absorption coefficient increases with the signal frequency, for each material there is a maximum frequency that can be utilized, beyond which the UT beam can not pass through the specimen. Furthermore the pulse-echo technique can be used only if the inspected

part has a thickness that is not so small as to avoid interference with the initial pulse and the first reflection of the opposite surface, nor too much larger as to cause a Back echo excessive attenuation even in samples lacking defects.

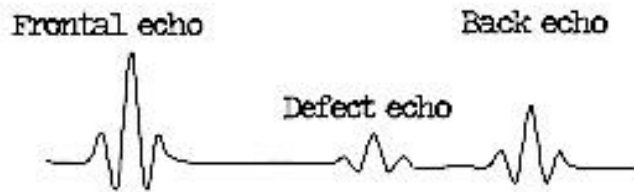


Figure 8. Ultrasonic complete waveform of a work piece containing a defect which correspond the Defect echo.

The UT NDE technique utilized for the applications discussed in this thesis work is a variant of the pulse-echo in which the UT beam is transmitted to the specimen after passing through a water layer where both probe and specimen are immersed (immersion scan). This variant is particularly indicated in the automatic scanning, as it allows for reciprocal and continuous displacements between the probe and the sample while ensuring constant coupling conditions; furthermore, working in immersion scanning is faster than contact method. Immersion scan techniques, however, require a bulky and expensive equipment. Moreover, as explained in the paragraph 2.3.3 Ultrasounds representations, the information from pulse-echo inspection can be displayed in different forms: A-Scan and B-Scan representations usually present the UT data on an oscilloscope screen; C-Scan, D-Scan and FV-Scan representations record the data by an x-y plotter and/or displayed/saved on a computer monitor/file.

2.3.2 Transducers

Probes and transducers are the UT NDE components apt to the UT signal generating, transmitting and receiving. In particular if a probe is both to transmit and to receive the ultrasonic waveforms, it is named Transducer. The transmitter probes transform the electrical impulses, received from the pulse oscillator/detector, into mechanical vibrations that generate the UT beam, while, the receiver probes make the inverse process, that is collecting the reflected UT waveforms (from the material) and converting them into electrical impulses. The piezoelectricity is the main phenomenon on which the transducer operation is based. It is the

property of some crystalline materials to polarize, if subjected to a mechanical deformation, generating a potential difference proportional to the mechanical deformation and, at the same time, to deform elastically if the opposite faces of the transducer are energized by electricity, generating a displacement proportional to the applied voltage, as shown in Figure 9.

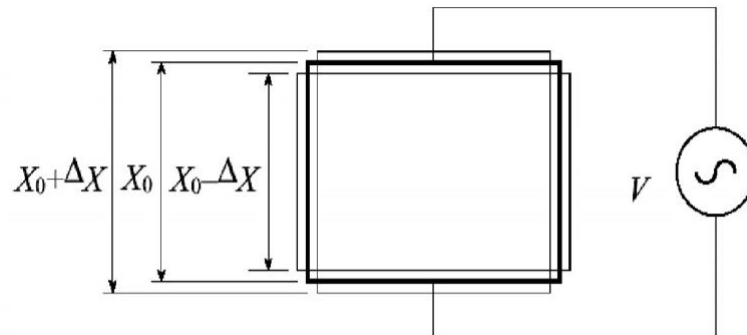


Figure 9. Piezoelectric crystal behaviour under voltage stress.

So the piezoelectricity allows to construct a probes that behaves both as a transmitter element and as a oscillator receiver.

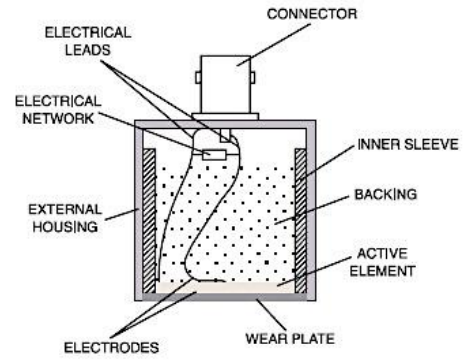
Exist two types of transducers:

- Normal beam probes - in which the ultrasonic beam is perpendicularly transferred to the material surface;
- Angle beam probes - in which the ultrasonic beam is angle transferred to the material surface (Figure 11);

Figure 10. (a) Straight beam transducer and (b) its scheme describes the structure of a generic straight beam probe consisting in a metal casing at bottom of which the disc-shaped transducer is fixed, within the enclosure there is an absorbent substance, whose function is to quickly damp the transducer oscillatory state. The transducer is metallized on the two opposite surfaces, so as to make possible the electrical connection to the terminals of the probe; the surface of the probe facing to the absorbent is connected to the central plug of the coaxial connector while the other electrode is connected to the coaxial connector corona through the metal detector casing.



(a)

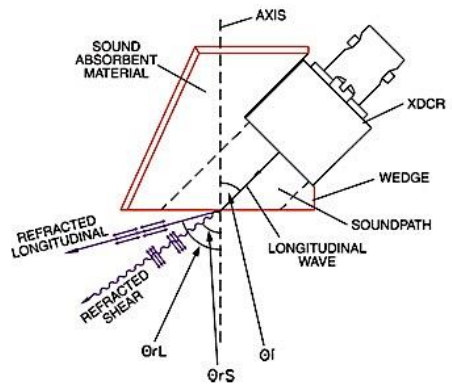


(b)

Figure 10. (a) Straight beam transducer and (b) its scheme.



(a)



(b)

Figure 11. (a) Angle beam transducer and (b) its scheme.

Regarding the transducers excitation, the voltage is impulsively transferred, generating in the probe the typical response of a damped system (Figure 12).

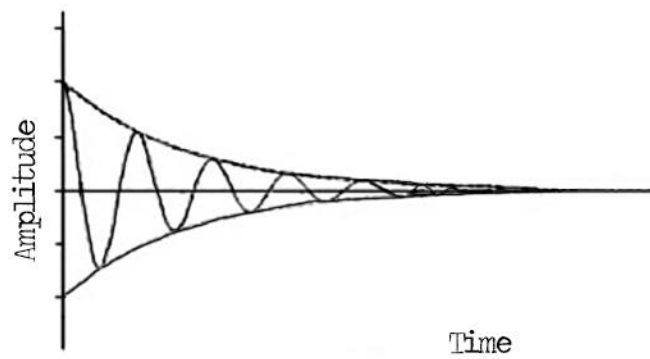


Figure 12. Damped response of a pulsed stimulate transducer.

These pulses are continuously sent into the material, out-of-phase of a certain time, so that when a pulse starts, the previous one is completely dissipated avoiding the presence of interferences in the response signals. Another possible differentiation is between the single transducer probes and the double ones. Figure 13 reports the section of a double transducer probe where it is possible to identify the two transducer elements (one receiver and the other transmitter), separated by an acoustically isolated septum. Each one is connected separately to the oscillator/detector with their respective coaxial cables. The surface of the sensor, made of Plexiglas, is designed to ensure good adhesion to the surface of the object.

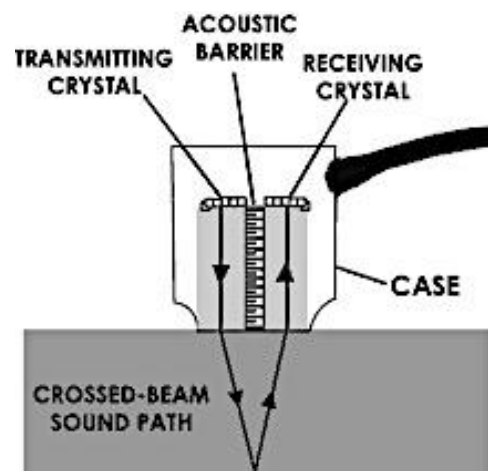


Figure 13. Section of a double transducer probe.

This type of probe, despite the single transducer model, has the advantage of the absence of the undesirable “dead zone” in the inspected material, that is the material part in which it is not possible to detect any discontinuities. In fact, once the UT waveforms are transmitted to the material, whenever a discontinuity is met, a part of them is reflected to the probe and if this part reaches the probe when it has not exhausted its forced oscillation, the oscillations of the reflected waveforms overlap with those still in transmission phase, making impossible to locate the defect. In other words the reflected beam must reach the probe after that the transducer returns in silence otherwise it will present a shadow area. Anyway the modern transducers eliminates the shadow area thanks to the complete separation of round trips. Last distinction can be made between focused and non-focussed UT probes. In particular the non-focused probe do not have the ability to focus the power emitted in a particular area, named focal zone, and the beam emitted is divisible in two zones called Near Field and Far Field. In the first zone, the beam diameter (whose radius is indicated by "r" in Figure 14) can be

considered approximately constant, while in the second zone it diverges at an angle α due to the phenomenon of volumetric dispersion so these probes are suitable for exploring a large area of the material.

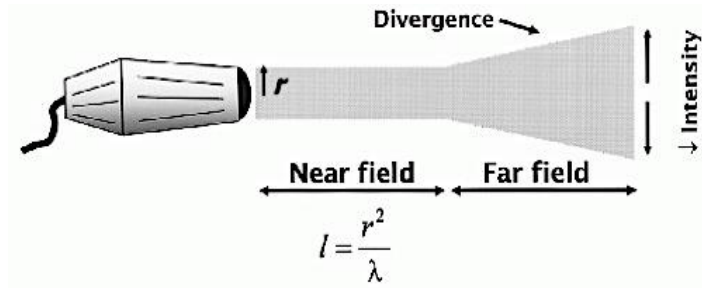


Figure 14. Non-focused UT ultrasonic beam.

The focused probes (Figure 15), instead, thanks to a focusing lens, are able to concentrate much of the power emitted in a limited area of space and therefore are best suited to a accurate exploration of the test sample but it is essential that the focal zone is in the centre of the sample.

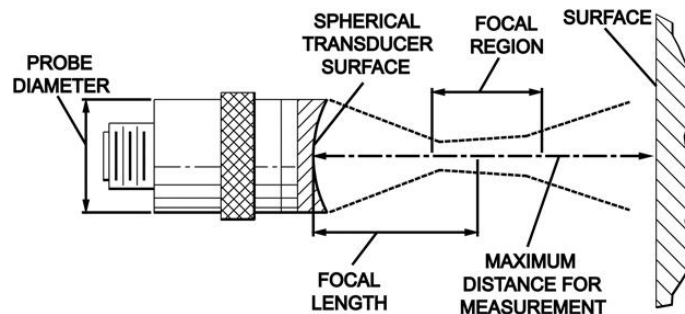


Figure 15. Focused UT probe scheme.

2.3.3 Ultrasounds representations

UT waveforms, once detected, should be represented in some way on a display device so that the operator can interpret the signal to evaluate the inspected sample material. For this purpose, representation methods (simple or complex) have been developed [25]. Below are described the known presentation methodologies.

2.3.3.1 A-Scan

A-scan display is basically a plot of amplitude versus time, in which a horizontal baseline on an oscilloscope screen indicates the elapsed time while the vertical deflections represent echoes (Figure 16). Defect size can be estimated by comparing the amplitude of a discontinuity echoes with that of a signal from a discontinuity of known size and shape. The depth at which a defect is located can be determined from the position of the first defect echo on the oscilloscope screen, moreover with a calibrated time base on the oscilloscope (horizontal scale), flaw location can be measured as the temporal distance between the echo relative to the UT signal entry in the upper surface of the sample (Frontal echo) and the position of the defect echo representing the UT signal travel within the sample material up to the defect. A-scan data can be displayed in the following two modes:

- radio frequency (RF) mode, in which the individual cycles comprising each pulse are visible in the trace;
- video mode, in which only a rectified voltage corresponding to the envelope of the RF waveform packet is displayed. This mode is suitable for ordinary ultrasonic inspection, but the RF mode is better for an optimum characterization of defects.

The A-scan display is not limited to the detection and characterization of defects; it can also be used for measuring thickness, or to obtain the UT velocities in materials of known thickness, or even for measuring the attenuation characteristics of specific materials, as well as for detecting the small cracks, porosity, and inclusions. It can be used with transmission or reflection techniques and it is almost always manually performed.

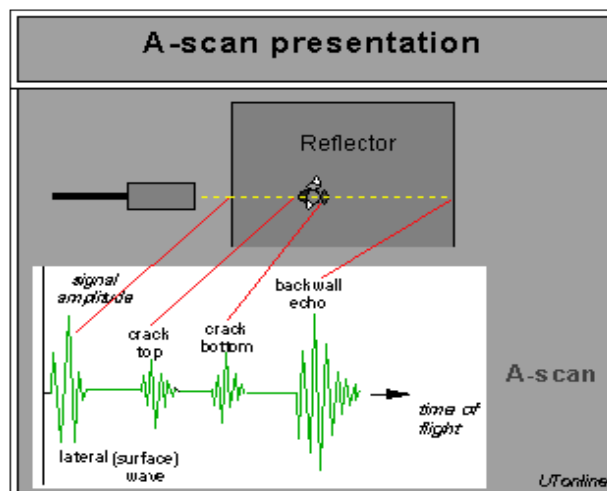


Figure 16. A-scan signal-inspection scheme.

2.3.3.2 B-Scan

B-scan UT representation is a x-y plot of time versus distance, that is the elapsed time vs the position of the transducer along the scanning line on the specimen surface. Echo intensity is not measured directly as it is in A-scan inspection, but it is often indicated semi-quantitatively by the relative brightness of echo indications on an oscilloscope screen. The presence of a reflected echo is detected by an event that is generated when the signal exceeds a predetermined threshold within a time gate set on the UT signal. This event is highlighted on the x-y diagram by a dot whose colour in a grey-scale or fake colour is proportional to the signal amplitude. The B-scan provides information about the depth and thickness of the defect for a single plane that normally intersects the specimen, arranged along the scan direction in other words a cross section of the specimen in correspondence of the scanning line. Moreover because the UT beam is lightly conical, defects near the Back specimen surface appear longer than those near the Frontal surface. The B-scan techniques have been more widely used in medical applications than in industrial applications. Optimum results from B-scan techniques are generally obtained with small transducers and high frequencies. In Figure 17 reported a scheme of the B-scan.

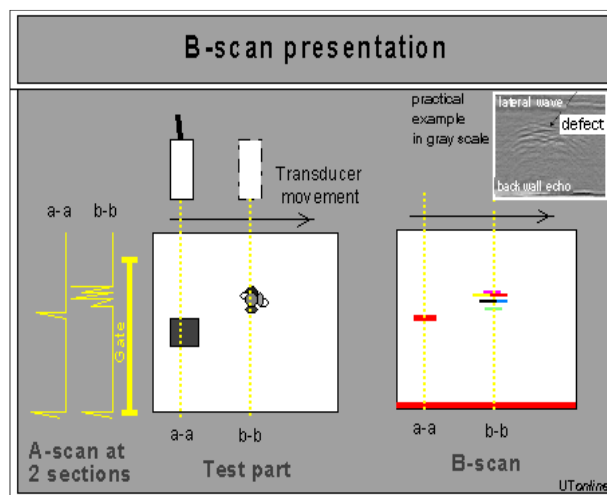


Figure 17. B-scan representation.

2.3.3.3 C-Scan

In the representation called C-Scan there is a two-dimensional (x-y) graph in Cartesian coordinates, in which the echoes generated by the discontinuities are mapped to the surface of the work-piece to be examined. As for the B-scan, the presence of a reflected echo is detected by an event that is generated when the signal exceeds a predetermined threshold within a time gate set on the UT signal. This event is highlighted on the x-y diagram by a dot whose colour in a grey-scale or false colour is proportional to the signal amplitude but differently from the B-scan in which is displayed a specimen section, in the C-scan a 2D projection of the internal structure of whole sample is represented (Figure 18). Moreover the advantage of the C-type representation is that it provides a visual indication of the defect for an easy and immediate interpretation. This type of representation can be accomplished by parameterizing both the signal amplitude and the flight time, obtaining in the first case a mapping of the signal fall, or the defect individuation along the test-piece thickness, in the second case. The limitation of this type of investigation lies in the lack of an adequate representation systems to determine the position of the internal discontinuity in the direction of the specimen thickness. Finally the size of a defect is estimated as a percentage of the scanned area.

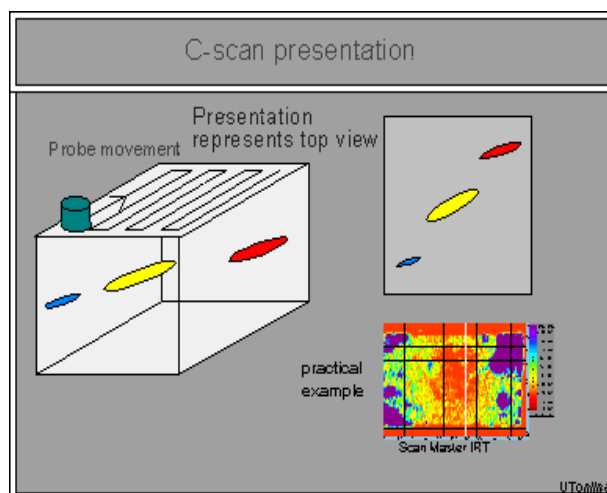


Figure 18. C-scan presentation (coloured circles are presenting areas of discontinuity).

2.3.3.4 D-Scan

The D-scan representation is a variant of the C-Scan in which the times of flight of the reflected echoes are reported instead of the amplitudes (Figure 19).

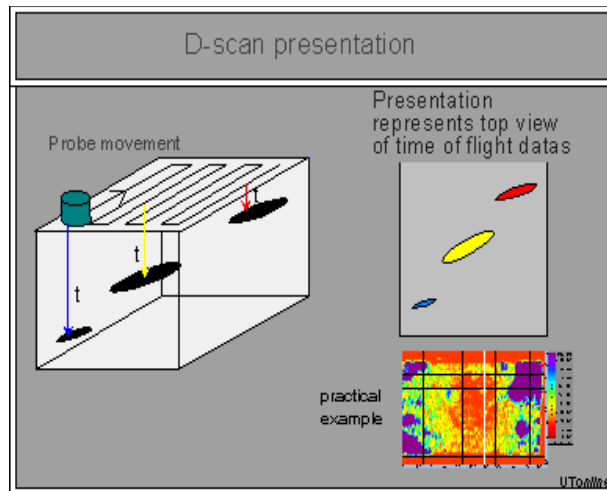


Figure 19. D-Scan representation.

2.3.3.4 FV-Scan

FV-Scan, or volumetric scanning, is a graphical representations consisting of a series of C-Scans in which depth information (z-axis) is also available for any discontinuities present. To have the information about the depth, in the thickness direction, this type of scan provide the detection of the complete ultrasonic waveforms and not only of their portion. In this way it is possible to generate ultrasonic images relative to the internal structure of different thick portions of the scanned specimen allowing the visualization of how the defect evolves in the sample thickness and the detection of the depth in which it has the maximum extension. This UT signal presentation is utilized for the applications here discussed. Moreover, the FV-Scan allow to measure the it also allows to measure the whole specimen thickness, knowing the UT propagation velocity within the material of the specimen, or otherwise it is possible to obtain the UT velocity by knowing the specimen thickness.

3. Advanced UT NDE scanning system

3.1 Introduction

The utilized advanced UT NDE system is composed by a purposely designed hardware configuration and a custom made software code, RoboTest© v.2.0, developed in LabView© at the Fraunhofer Joint Laboratory of Excellence on Advanced Production Technology, Naples, Italy [31]. The system is designed to perform different types of UT acquisitions: simple scan (C-scan), adaptive scan (for the samples with complex geometry) and FV-scan. In this chapter the ultrasonic (UT) full volume (FV) scanning procedure based on pulse-echo immersion testing and the processing of the resulting UT volumetric data file are illustrated.

3.2 Scanning system hardware components

The UT NDE system used for the applications discussed in this thesis work consists of the following hardware components:

- Generator/Detector of ultrasounds: Krautkrämer USIP 12
- Digital oscilloscope: LeCroy 9400
- Handling system: Stäubli RX 60 L + controller CS7B
- Control station: Personal Computer with:
 - National Instruments board: PCI-GPIB IEEE-488.2
 - Ethernet interface data transfer velocity: 10-100 Mbit/sec

In Figure 20 the operating scheme diagram of the utilized UT NDE system is reported. In particular, as explained in general in the paragraph 2.3.1 Scanning techniques about the pulse-echo technique, during a scan the temporal sequence of the events is:

1. A custom-made software, running on the PC, forwards, through Ethernet interface and FTP protocol, the movement commands to the controller (which function is to handle the anthropomorphic arm and consequently to displace the UT probe),
2. The UT generator/detector sends electric pulses to probe stressing the piezoelectric crystal (contained in the probe) and generates an UT waveforms

3. The generated UT waveforms travel from the probe to the sample and the reflected part came back to the probe (following the reverse path)
4. The reflected and returned UT waveforms stress mechanically the piezoelectric crystal that generates electric pulses
5. The analogic electric pulses are sent to the generator/detector who, in turn, sent them to the digital oscilloscope
6. The digital oscilloscope converts the analogic UT signal into a digitalized one and sent it to the custom-made software (through GPIB interface and the communication protocol 488)
7. The received digitalised UT signal is saved in a data file together with its relative coordinate information
8. Finally the created UT data file, also later, is processed by the custom-made software to generate ultrasonic images of the internal structure of the scanned material.

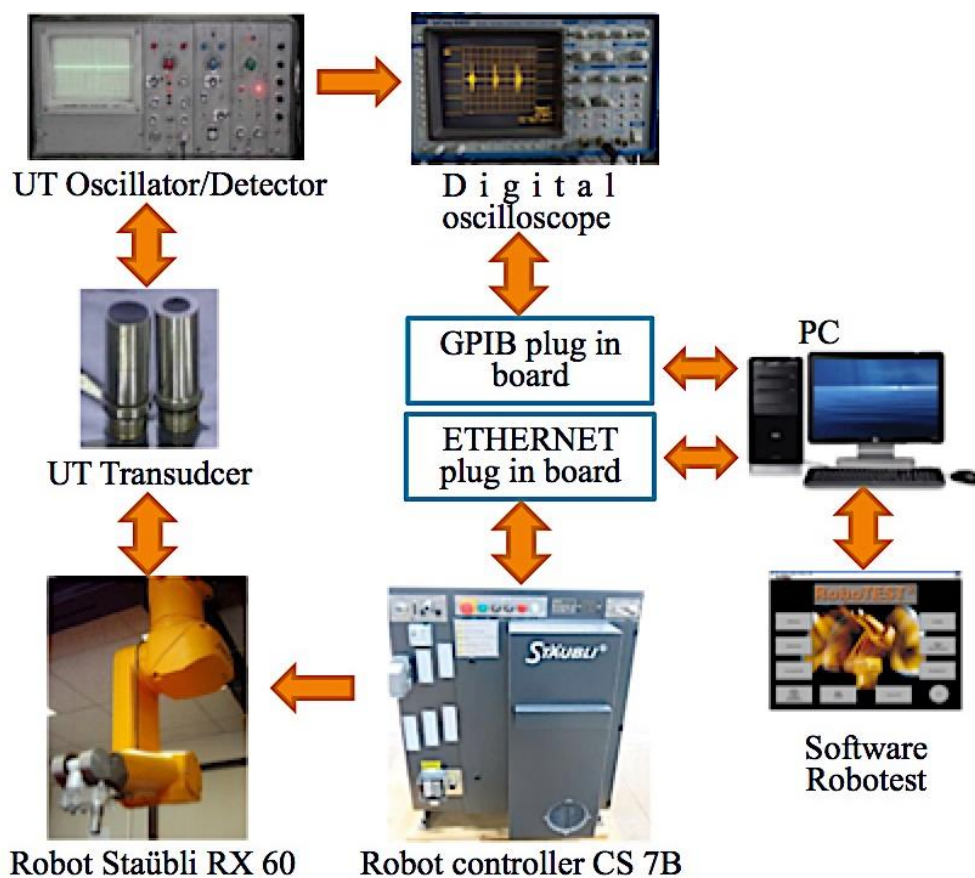


Figure 20. Utilized UT NDE system components/scheme.

3.2.1 UT oscillator/detector

The Krautkrämer USIP 12 (Figure 21) is the “heart” of the UT inspection because it has the dual tasks to emit and send electrical impulses to the transducer for their transformation into UT waveforms, and simultaneously the function to receive and amplify the return signals. It is also capable to perform preliminary analysis on UT signal to eliminate the Background noise and the electrical noise. Moreover it has the following functionalities [32]:

- GATES FUNCTION - select and transfer to the oscilloscope only the selected signal portion
- FA - Frequency Analysis – to hang up, through a hardware trigger, the peak of the waveform relative to the interface of the examined specimen
- RF - Radio Frequency – to view and download the complete ultrasonic waveform



Figure 21. Krautkrämer USIP 12.

3.2.2 Digital oscilloscope

The LeCroy 9400 is a digitizer oscilloscope capable of sampling input signals and showing them on a cathode-ray detector for any regulation such as the time scale adjustments (x axis), or signal amplitude (y axis). It is equipped with two input channels, each one with an 8-bit analogue/digital converter and 32 Kbyte acquisition memory, with maximum sampling rate of 100 MHz [33]. By setting two cursors the LeCroy 9400 automatically returns the time interval between two echoes of the ultrasonic displayed waveform. The peculiarity of this oscilloscope is that it has a 9-pin serial output and a faster GPIB output more reliable than the previous

ones, for personal computer connections with their respective ports. This latter feature makes it particularly suitable for remote control for computer-assisted measurement applications or automated tests because the entire measurement process, including changes to the Frontal panel settings, can be controlled via the GPIB port from the remote PC at a data transfer rate of over 400 KB/s, thanks to the IEEE 488 communication protocol, or of 7 MB/s, if it is used the HS 488 protocol.

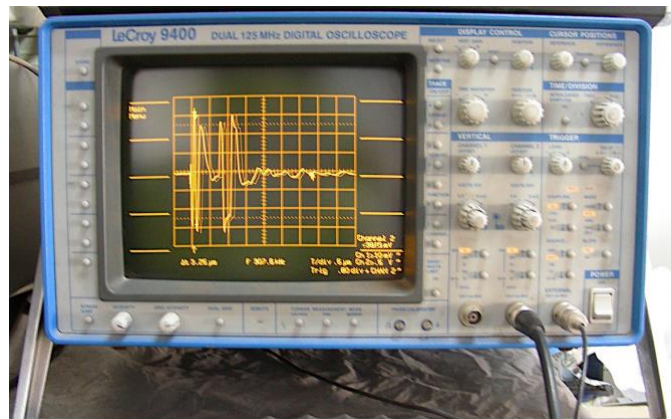


Figure 22. Digital oscilloscope LeCroy 9400.

3.2.3 UT transducer

The transducer utilized for the UT scanning performed on the three applications is a transmitter/receiver focused high frequency (15 MHz) UT immersion probe for pulse-echo testing (Figure 23).



Figure 23. Focused high frequency probe.

3.2.4 Mechanical UT probe displacement system

The mechanical system for probe displacement during an ultrasonic scanning is composed by an anthropomorphic robot and its controller. The anthropomorphic robot is the Stäubli RX60L and it has a spherical wrist that allows to position and orient the ultrasonic transducer in three-dimensional Cartesian space and in a precise and fast way. The anthropomorphic geometry is achieved with three rotoidal joints: the first joint is called "foot"; the second is named "shoulder" joint due to its resemblance to the human arm; while the third joint, that constituted the connection between the "arm" and the "forearm", is named "elbow" joint. The structure of the manipulation is responsible of wrist positioning task allowing to orient the terminal organ. The spherical pulse has three freedom degrees realized by rotoidal joints and it permits an arbitrary orientations in a three-dimensional space. The anthropomorphic structure is the most agile manipulation structure, thanks to the presence of all rotoidal joints but the mobility and freedom degrees are completely lost and the wrist positioning accuracy changes throughout the work space (approximately a portion of sphere). The RX60L can achieve the maximum distance of 865 mm with a repeatability of 33 micron and accuracy of about 50 microns. The maximum Cartesian speed is 1.8 m/sec while the nominal payload is 1.5 Kg [34]. The arm can be mounted depending of necessity, for example on the floor, on the wall or, as in our case, on the ceiling through two steel girders. The arm end with a flange to which the chosen ultrasonic probe can be fixed. The second component of this mechanical system is the controller that is constituted by: the Stäubli CS7B control cabinet, the programming terminal and by the learning base (MCP). The control cabinet (the intelligent part), drives the robot through numeric power amplifiers dedicated to each of the six axes of the arm [35]. The conversion of electric energy is ensured by a power block that provides the required voltage to each one of the mentioned elements to ensure its proper operation. The controller is made up of:

- central unit that controls the peripheral device:
 - flash disc,
 - serial gateways,
 - Ethernet gateway,
 - user interface
 - board "interface AWC"

- an axis interface board with motor control amplifiers
- other optional boards

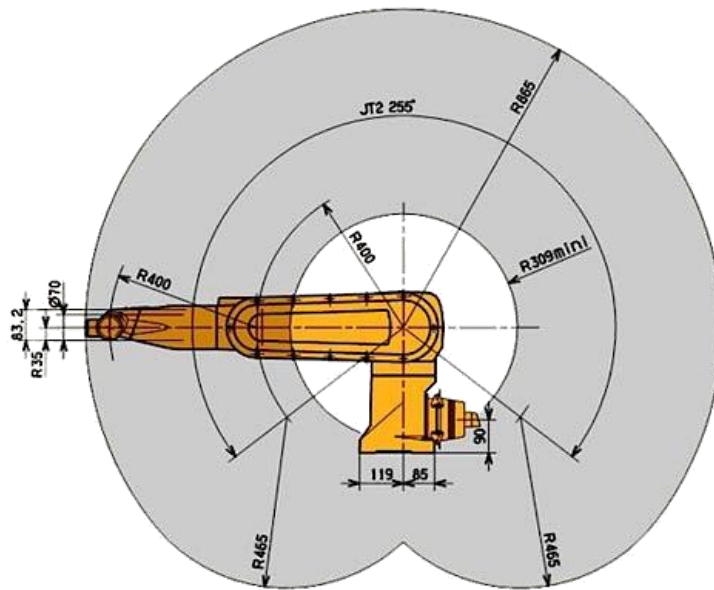


Figure 24. RX60L work volume.

The AWF interface board groups all the signals that ensure the safety motion of the arm and part of the input/output signals, and it also provides to the numeric amplifiers the reference signals for controlling the feedback current and the speed of the assignments. Numeric amplifiers provide power to the motors depending on the controls received from the axis control board and report to the controller the position information of the motors. This information is an incremental positions information in fact the real position is determined from an absolute starting position. The learning pad allows manual control of the robot. The alphanumeric terminal consists of a 14 inch cathode-ray monitor and a keyboard with which you can enter data and programs into the robot's memory.

3.2.5 Personal computer

The personal computer is essentially dedicated to execute the custom-made software to automate the motion control system through the Ethernet board, to set up and acquire UT waveforms from the digitizer oscillator through the GPIB port, and to save and store the ultrasonic scanning files on the hard disk. The PC technical characteristic are:

Motherboard	IBM compatible with chipset SiS 645
Processor	Intel Pentium4, 2500 MHz
RAM	512 MB, DDR 400 MHz, PC-3200
HDD	EIDE, ATA-133, 200 GB, 7200 rpm, 8 MB cache
Graphic card	ATI Radeon 256 MB, 128 bit
Optical drive	CD Writer DVD-RW
Floppy player	3,5 inch
Ethernet Board	Realtek 10/100 MB/s
GPIB Board	NI PCI-GPIB 488.2
Monitor	LCD Acer 19", 8 ms
Operative System	Microsoft Windows Xp Professional SP2

Table 1. PC characteristics.

Nowadays this PC is quite similar to any other office computer due to the rapid obsolescence of the electronic components characteristic. The PC has only one infinite queue regulated by FIFO logic (First In First Out) and with an exponential distribution of the arrival data and an inter-arrival frequency equal to 3 points per second. Moreover, thanks to the used HS 488 protocol, which offers data exchange rates close to 7 Mbit/sec, and thanks to the disk cache memory (with access times of about 12 ms), queue response times small in 99% of cases were obtained, confirming that the PC is well dimensioned for this UT NDE system.

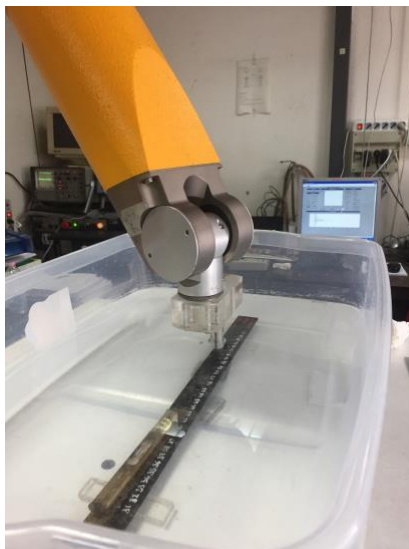
3.3 UT FV scanning procedure based on pulse-echo immersion testing

The UT FV scanning procedure based on pulse-echo immersion testing was utilized to perform the UT scans (Figure 25 (a)) on the samples under examination. The terms Full Volume indicates that the acquired waveforms are complete ultrasonic waveforms, this allows to have the information relative to the whole thickness of the examined sample and to make possible the generation of ultrasonic images relative to the internal structure of the specimen material through the sub-module Ecus Inspection© of the software Robotest© (see next paragraph). While the terms “pulse-echo” mean that the reflection method is used [25], and

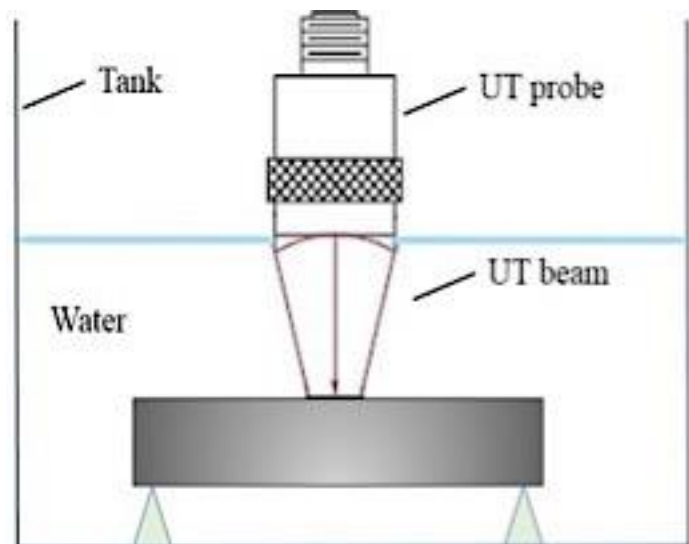
“immersion” that the inspected sample and the ultrasonic probe are both immersed in a coupling medium (water in this case) as shown in (Figure 25 (b)), moreover the utilized probe is a focused transducer, both transmitter and receiver. Following the main scan parameters to be set are reported below:

- Control Technique: Full Volume (FV-Scan)
- Scan method: Pulse-echo (Reflection), immersion
- Probe type:
- Oscilloscope set-up:
 - Sampling rate
 - Visualization parameters
 - Gain and Damping
- Scan area: depends on the applications
 - # X Steps: depends on the scan area
 - # Y Steps: depends on the scan area
- Scan step (0.1 minimum step)

The duration of each scanning was about 1 hour because of the chosen scan step is the smallest one.



(a)



(b)

Figure 25. UT FV scanning procedure based on pulse-echo immersion testing (a) execution and (b) its scheme.

3.4 UT signal acquisition and processing software

In the following paragraphs the custom-made software, Robotest©, and its sub-module, Ecus Inspection©, will be illustrated. In particular, as you will see, Robotest© is apt to control the UT NDE system and to perform the UT FV scanning procedure based on pulse-echo immersion testing, while Ecus Inspection© is dedicated to the processing of the resulting UT data in order to generate single or multiple UT images of any thickness portion of the internal structure of the sample material under examination.

3.4.1 Custom-made software – Robotest©

Robotest© is the custom-made software, developed in LabView© v5.0 environment at the Fraunhofer Joint Laboratory of Excellence on Advanced Production Technology, Naples, Italy [31], dedicated to control the ultrasonic scanning system and to perform different types of UT scanning. In order to realize the three applications carried out for this thesis work, Robotest© was upgrade to LabView© version v16.0 and, thanks to enhancement of new version v16.0, same error corrections were made and same improvement and new functionalities, were added to the custom-made software, which have resulted in better stability of whole system. In general an UT scanning consists in a step-by-step sample investigation and in the identification and acquisition, for each scanned point (e.g. for each step), of a number of Volt values (depending on the sampling rate) that correspond to the UT waveform values. Robotest© is capable of driving the six-axes anthropomorphic robot RX60L (from Stäubli) and, at the functional level, of acquiring ultrasonic complete waveforms, saving them in appropriate volumetric file (in *.DAT format) and then processing the created file to generate single or multiple ultrasonic images in grey scale or fake colours of any thickness portion of the internal structure of the investigated specimen. The main menu of Robotest© (Figure 26) presents different buttons to lunch the diverse types of scanning (Simple Scan, Adaptive Scan, Full Volume Scan), to appropriately calibrate the instrumentations (Robot Manual Control, Oscilloscope, Manual Distance and Thickness Measurements) and to choose the graphic processing to be made. The mentioned functions, accessible from the main menu, are briefly explained below:

- **Adaptive Scan**: Starts the scan for the acquisition of specimen geometry
- **Full Volume Scan**: Starts the full scanning for the UT signal acquisition
- **Simple Scan**: Starts a complete scan without the preliminary Adaptive Scan
- **Manual Distance and Thickness Measurements**: Starts the virtual instruments for the thicknesses and distances manual measurement
- **Robot Manual Control**: Shows the robot Stäubli RX60L control panel
- **Oscilloscope**: Shows the digital oscilloscope LeCroy 9400 control panel
- **2D Image**: Starts the program for the 2D images generation
- **3D image and Surface Profiling**: Starts the program for the 3D images generation Ecus Inspection©
- **Quit**: Stop the the software execution

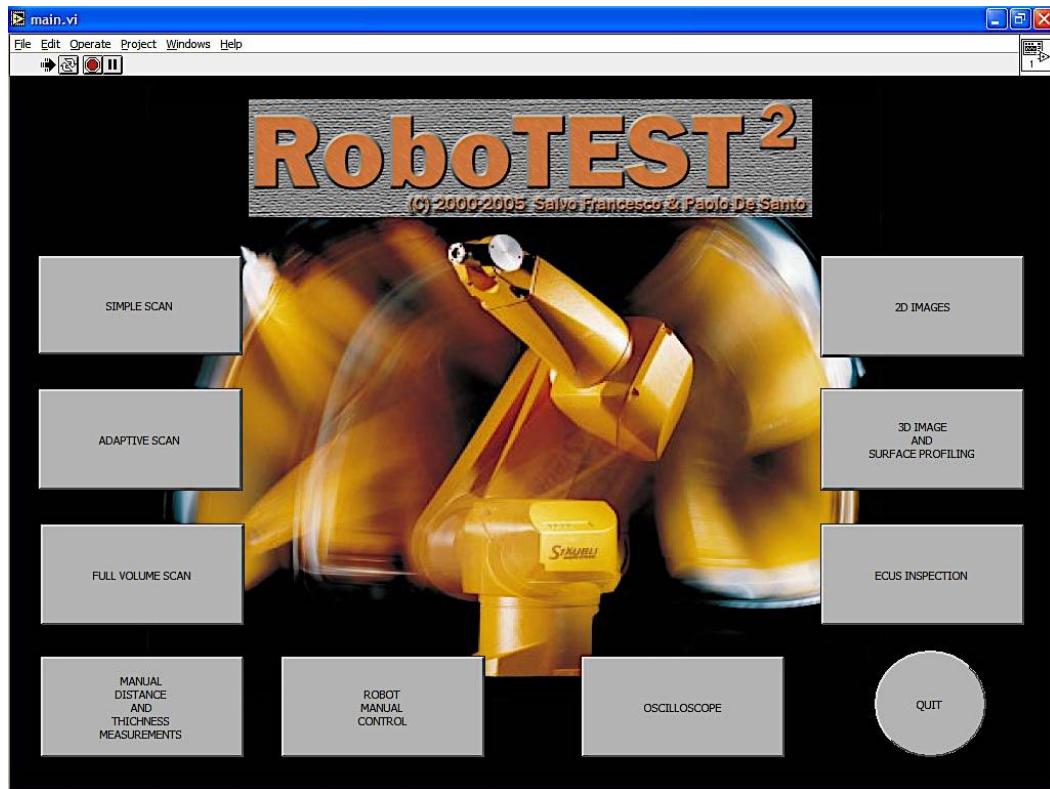


Figure 26 Software Robotest© main menu.

In Figure 27 is reported the user interface of the Robotest© sub-module dedicated to perform the Full Volume simple scan (or flat scan).

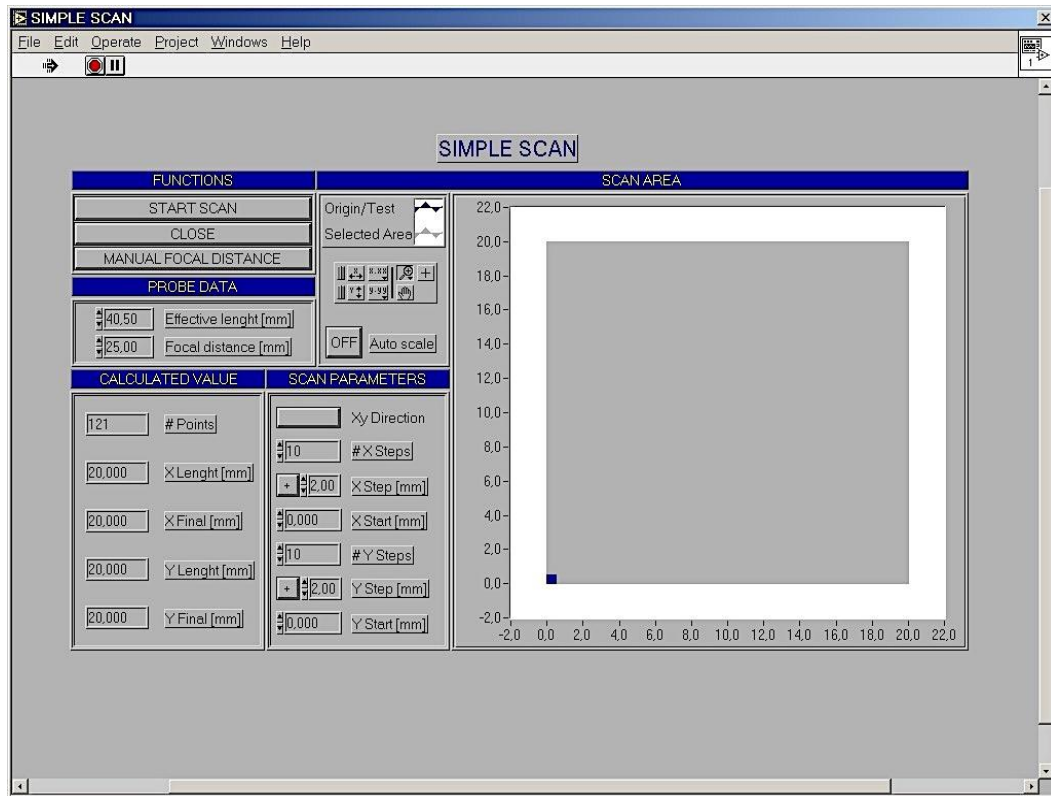


Figure 27. Full Volume Scan user interface.

The parameters to be insert are:

- Scan direction (Xy direction or xY direction)
- Number of steps on x axis (# X Steps)
- Step dimension on x axis (X Step)
- Number of steps on y axis (# Y Steps)
- Step dimension on y axis (Y Step)
- Initial scan point (X Origin and Y Origin)

These parameters identify the rectangular area of the specimen on which the FV simple scanning will be performed, in fact the box "Scan Area" displays graphically the scanning area with a grey rectangle and the axes origin with a little blue square on the graph. The axes origin coincides with the "test" point, that is, the point where the distance measurement between the probe and the surface to be inspected is performed. In particular the test point must be easily identifiable on the surface of the specimen, sufficiently distant from evident surface defects and from the edges of the specimen. The positioning of the probe at right focal distance can be performed manually or automatically (through "Manual Focal Distance" or

“Auto Focal Distance” buttons). After the setting of the focal distance you can start scanning through the "Start Scan" button but before the scanning start the “SETUP ROBOT STÄUBLI RX60L” user interface appears (Figure 28) to set other functionalities for the complete control of the robot [26].

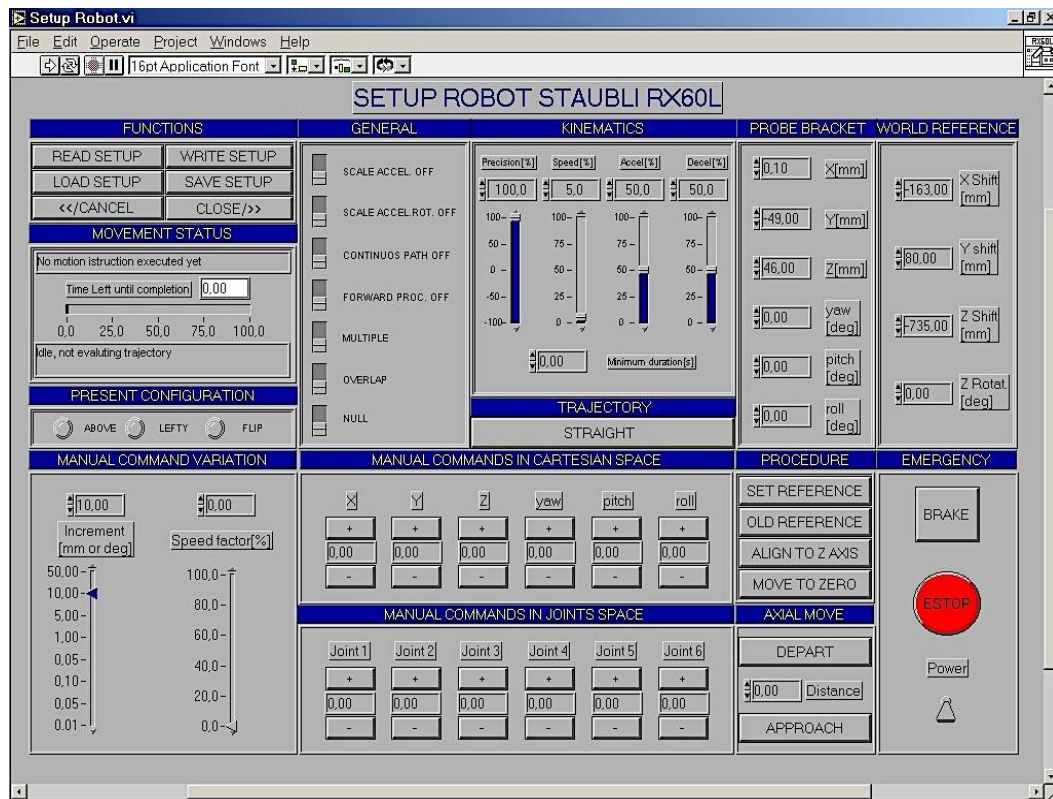


Figure 28. Set-up RX60L user interface.

3.4.2 Ecus Inspection© – UT images generation

Ecus Inspection©, as introduced in the previous paragraph, is the sub-module of the Robotest© dedicated to processing the UT volumetric *.DAT file, containing the complete UT waveforms detected during the Full Volume scanning, in order to generate single or multiple ultrasonic images of any thickness portion of the internal structure of the sample material. In the Figure 29 you can see the first user interface that appears when push the “Ecus Inspection” button from the Robotest© main menu. First a pop-up opens to choose the path where the UT volumetric data file you want to open is located, then the user interface appears presenting the following elements/functionalities:

- 2D scheme of the scanned area with a red mobile cursor that allows to select any scan point, reporting its (x,y) coordinates, and to retrieve the relative UT waveform
- XY graph where is reported the single waveform chosen, through the red slider, where the ordinates are the normalized values of the waveform (ranging from 0 to 255) and the abscissas are the samplings number
- Main scan information: number of points inspected along the two directions (X, Y), scan step size, check boxes to choose the further analysis (e.g. “Single Image”, “Change Limits”, “Multi Image”, etc.)

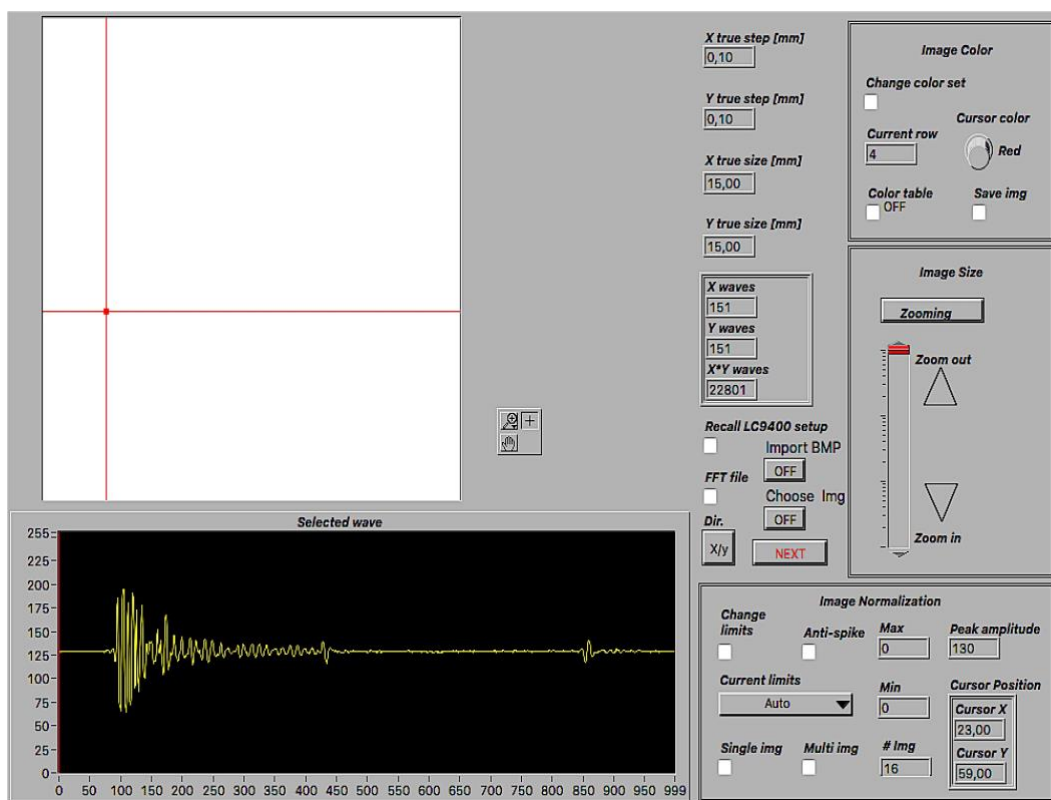


Figure 29. First Ecus Inspection© user interface.

Opened the data file an ultrasonic complete waveform must be selected by moving the red cursor on the 2D scanned area scheme, then clicking on the check box “Change Limits” a second user interface opens where the selected waveform is represented in a Volt/Division graph (e.g. Volt on the Y axis and Time of Flight (seconds) on the X axis). In order to obtain the 2.5D axial tomography of the sample under examination a time-gate on the displayed waveform needs to be set through two vertical cursors (Figure 30), and the number of sub-gates

can be choose ranging from 1 to 16. Then, clicking on “Multi Image” check box, Ecus Inspection© will generate an UT image for each time sub-gate. Moreover, as the time axis orientation corresponds to the UT waveforms propagation in the sample thickness direction, the time sub-gate width identifies the thickness portion to be imaged, therefore each UT image corresponds to the internal structure of the sample thickness portion identified by the relative time sub-gate.

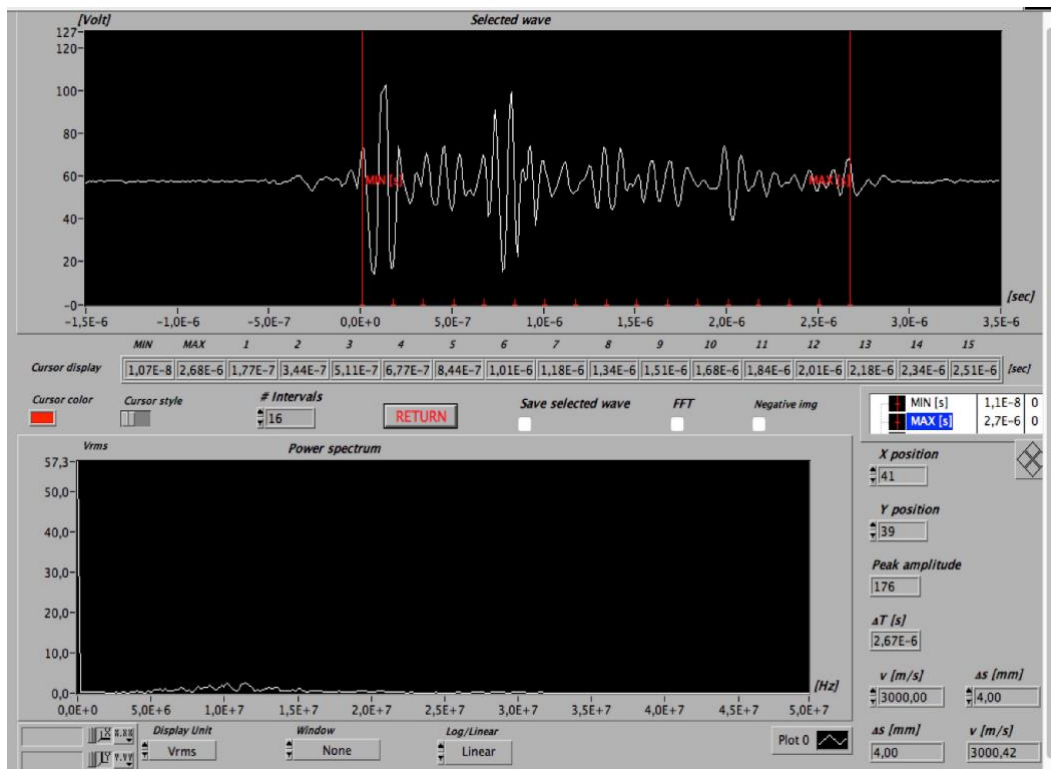


Figure 30. “Change Limits” user interface: selected UT waveform and its sub-gates.

In the Figure 31 is reported an example to better explain the correspondence between each time sub-gates and the relative specimen thickness portions, which, in turn, correspond to the UT images of the sample material internal structure. In particular the Figure 31 shows a typical complete UT waveform, relative to an UT FV scanning performed on a specimen containing a defect. Observing the UT signal you can identify the presence of the following three echoes (starting from the left to the right):

1. The Frontal echo, relative to the UT waveform reflection by the interface between the water and the upper specimen surface, represents the beginning of the specimen

2. The Defect echo, relative to the UT waveform reflection by the specimen/defect interface, represents the depth (in the thickness direction) at which the defect appears
3. The Back echo, relative to the UT waveform reflection on the interface between the last specimen surface and the water, represents the end of the specimen thickness

In general the first image, relative the sub-gate set on the Frontal echo, represents the entrance of the UT waveform into the sample material while the last image, relative to the sub-gate on the Back echo, represents the exit of the UT waveform from the sample material and correspond to a C-Scan of the specimen, that is the projection of its whole internal structure.

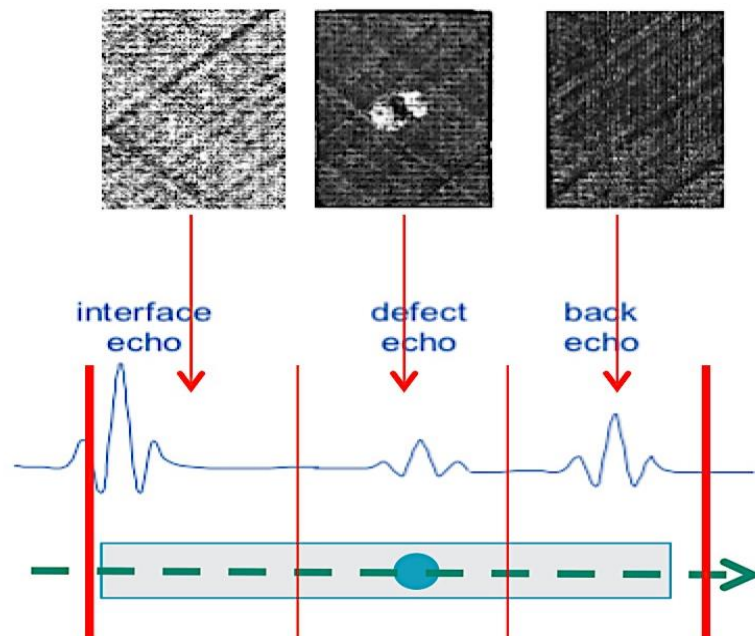


Figure 31. Example of a complete UT waveform with three sub-gates and relative UT images.

In Figure 32 other example of 16 UT images relative to an impacted CFRP laminate is reported, where because the time-gate was set to the whole UT signal and it was divided into 16 equal sub-gates, each generated UT image corresponds to one sixteenth of the sample thickness.

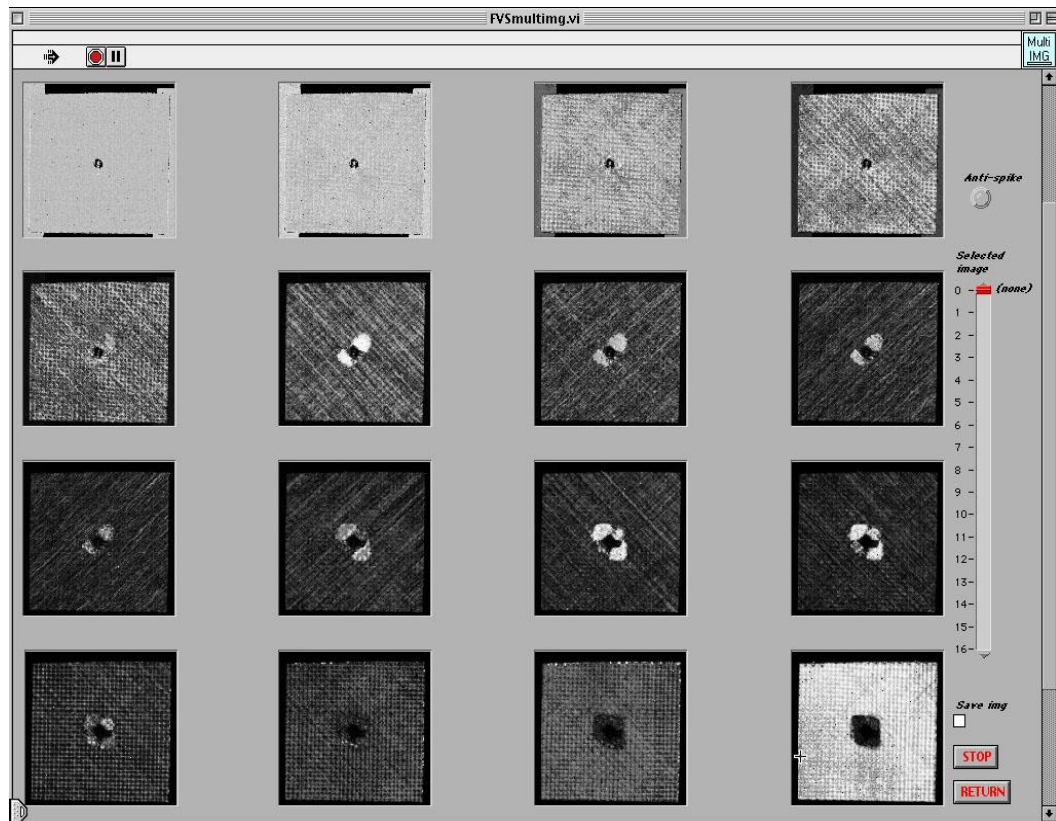


Figure 32. 16 UT images of an impacted CFRP laminate. Each image corresponds to 1/16TH of the laminate thickness.

The FV UT scans allow to perform a non-destructive accurate evaluation of the goodness of the internal structure of the examined laminate as well as the quantification of its precise thickness, not least the orientation of the various carbon fiber layers. In addition, UT images can be used to study the presence and geometry of delaminated areas as well as their development in the laminate thickness direction and to connect the extent of delamination damage with the impact energies intensity.

4 UT NDE case studies

4.1 Introduction

In this chapter, the applications of the illustrated advanced UT NDE system are presented. Three diverse CFRP aeronautical components were subjected to an UT FV scanning procedure based on pulse-echo immersion testing. In particular:

- a custom-made software code Robotest© developed in LabView environment was utilized for UT probe displacement using a 6-axis robotic arm
- a sub-module Ecus Inspection© was used for UT images generation and analysis
- a custom-made software was properly developed in Matlab® environment for the 3D thickness reconstruction of the defects

The first case study is focused on the UT inspection of CFRP non-crimp fabric (NCF) laminates allowing a metrological characterization of a CFRP NCF not impacted laminate, and a quality assessment of CFRP NCF impacted laminates (with different impact energies).

The second case study regards the quality assessment of the bonding process of CFRP adhesive bonded joint laminates in terms of adhesive layer homogeneity evaluation and 3D thickness reconstruction (both adhesive layer and entire bonded joint laminates).

The third and last case study concerns the quality assessment of the drilling process of CFRP drilled laminates in terms of drilling process evaluation and push-out delamination characterization through a 3D thickness reconstruction.

4.2 Case Study n° 1 – Metrology characterization and quality assessment of CFRP non-crimp fabric laminates

The first case study is focused on two different analysis executed on CFRP non-crimp fabric (NCF) composite laminates comprising of:

- 1) metrological characterization of not impacted CFRP NCF laminates in order to verify:
 - a. the correct stacking sequence
 - b. the single layers and the total laminates thicknesses

- 2) quality assessment of impacted CFRP NCF laminates in terms of:
 - a. damage transition in the stacking sequence analysis
 - b. damage position in the thickness direction calculation

These analysis were carried out performing the UT FV scanning based on pulse-echo immersion testing on the NCF laminates, processing the resulting UT volumetric data file by the custom-made software Ecus Inspection© and observing the generated UT images relative to the internal structure of the laminates material.

4.2.1 CFRP material

The CFRP samples under examination are 4 mm thick non-crimp fabric (NCF) quadriaxial laminates (Figure 33) fabricated using resin infusion under flexible tooling (RIFT) technology [36, 49]. The benefit of NCF composites employment is that their fibers are not crimped and one macroscopic layer (which consists of different sub-layers) can be processed instead of several sub-layers [37]. In the RIFT process, reinforcing fibers are first placed on a female mould and then a flexible tooling coating is placed over the fibers and sealed around the edges in vacuum tight manner [38]. The resin is drawn in the mould by vacuum action and impregnates the preform. The shape of the part is obtained by vacuum infusion of the fibers between mould and flexible tooling coating [30]. Quadriaxial laminates were manufactured with the following symmetrical stacking sequence: [+45°/0°/-45°/90°, +45°/0°/-45°/90°, 90°/-45°/0°/+45°, 90°/-45°/0°/+45°]s. The plastic matrix was Hexcel HexPly®M36 epoxy resin

and the carbon fibers type was Tenax HTS 5632 12k. Polyester stitching yarn (50 dtex) was used for joining with 2.5 mm stitch length. Final fiber aerial weight per single orientation layer was 267 g/m² and fiber volume fraction was 62%. Rectangular specimens of 100 mm x 150 mm size were cut from the manufactured laminates (Figure 33).

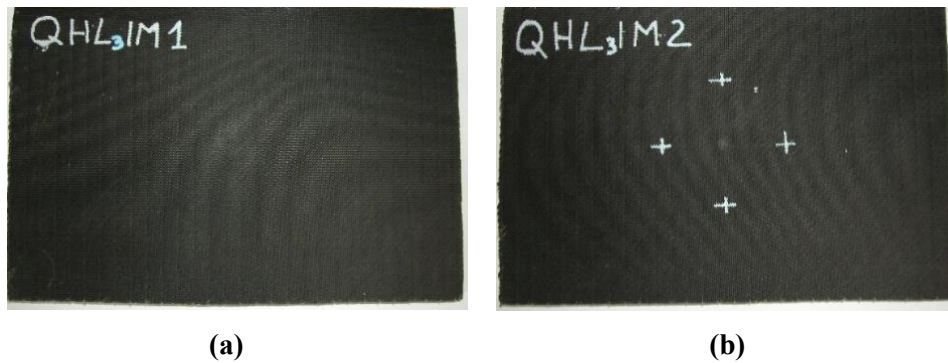


Figure 33. (a) Not-impacted “QHL3IM1” laminate and (b) impacted “QHL3IM2” laminate.

4.2.2 Impact testing

Dynamic impact tests [39] were performed through a CEAST Fractovis MK4 falling weight machine (Figure 34) using a cylindrical indenter with hemispherical nose (Figure 35). NCF composite rectangular specimens were clamped in an appropriate fixture (Figure 36). The Das 4000 dedicated software was used for impact test data recording.



Figure 34. CEAST Fractovis MK4 falling weight machine.



Figure 35. Cylindrical indenter with hemispherical nose.

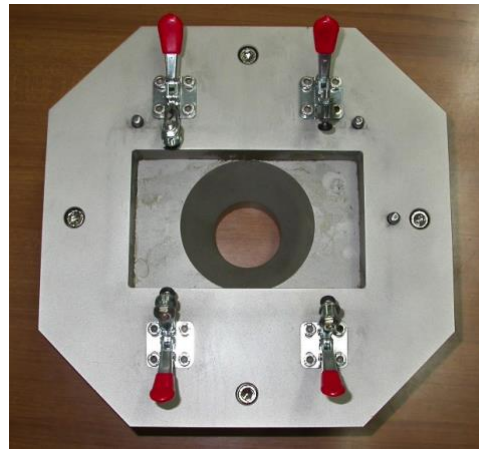


Figure 36. Appropriate fixture to clamp the rectangular specimens.

Diverse impact energies were employed for the testing campaign: 9, 12, 16, 20, 25, 30, 40 J. In Table 2, the selected parameters for the impact testing plan are reported.

Samples ID	Height (m)	Mass (kg)	Impact energy (J)	Speed (m/s)
QHL3IM1	-	-	-	-
QHL3IM2	0.255	3.6	9	2.24
QHL3IM3	0.340	3.6	12	2.58
QHL3IM4	0.453	3.6	16	2.98
QHL3IM5	0.567	3.6	20	3.33
QHL3IM6	0.708	3.6	25	3.73
QHL3IM7	0.546	5.6	30	3.27
QHL3IM8	0.728	5.6	40	3.78

Table 2. Parameters of the impact testing plan.

4.2.3 UT FV scanning based on pulse-echo immersion testing of CFRP NCF laminates

The UT FV scans were executed on eight CFRP NCF laminates (one not impacted laminate and seven impacted laminates) with the following settings:

- Focused high frequency transducer (15 MHz) with focal length equal to 49.6 mm
- Oscillator/detector set at 90 dB gain and medium damping
- Digital oscilloscope set at 1 V (Volts/div), 0.5 μ s (Time/div) and 100 MHz sampling frequency, resulting in 500 samplings for each detected UT waveform
- Scan step: 0,1 mm (following a boustrophedonic raster scan)

The scanning area was 11 mm x 15 mm for each of the 7 NCF laminates. The duration of each scan (for the above scanning area) was about 1 hour.

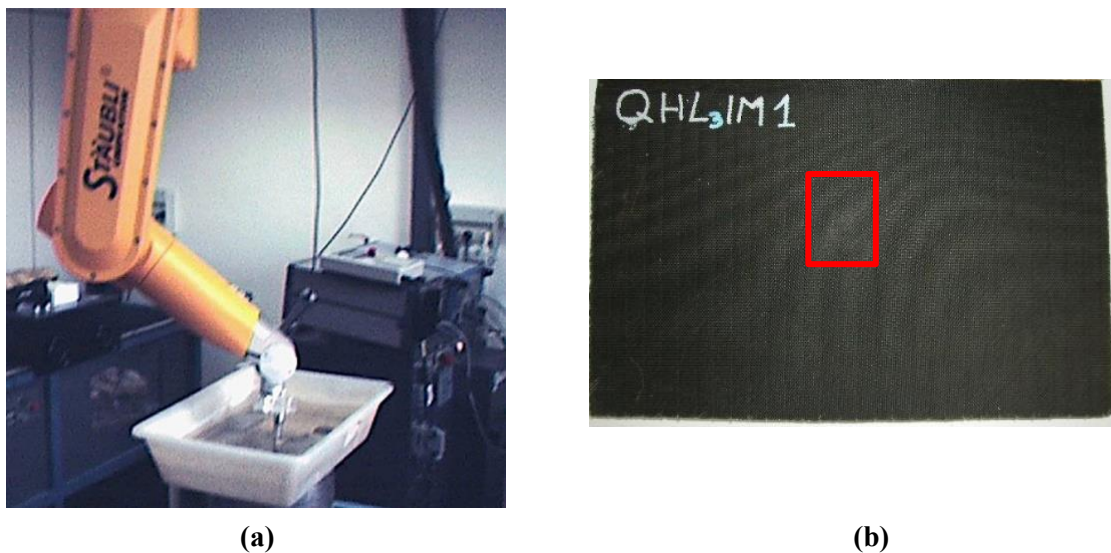


Figure 37. (a) UT FV scanning of the CFRP NCF laminate; (b) scanned area 11 x 15 mm.

4.2.4 Metrological characterization of the CFRP NCF laminate

As mentioned in the chapter introduction, the metrological characterization on the first quadriaxial CFRP NCF not impacted laminate (QHL3IM1) consists of:

- a. correct stacking sequence evaluation
- b. single layers and total laminates thicknesses calculation

4.2.4.1 Correct stacking sequence evaluation

The correct stacking sequence evaluation was carried out through the sub-module Ecus Inspection© by processing the UT volumetric data file resulting from the UT FV scan and by examining the UT images generated for each single fiber layers of the NCF laminate. The first user interface (Figure 38) shows the 2D scheme of the scanned area from which, moving a cursor, a typical UT waveform has to be selected and retrieved. Then, clicking on the check box “Change Limits”, a second user interface appears (Figure 39) where the time gate and the relative time sub-gates have to be set in order to identify the number of UT images to generate. Hence, in order to evaluate the correct stacking sequence and knowing that the laminate is composed by 16 unidirectional fiber layers (nominal thickness = 0.25 mm), it is easy to understand that the number of the time sub-gates needs to be set is equal to 16 (Figure 39). Moreover, as the time axis orientation corresponds to the UT propagation in the laminate thickness direction, each time sub-gate width identifies the thickness portion to be imaged. Consequently, each of the 16 UT image (generated from the 16 time sub-gates) will properly correspond to 1/16th of the laminate nominal thickness. Finally, clicking on the check box “Multi Image”, the 16 UT images were generated (Figure 40).

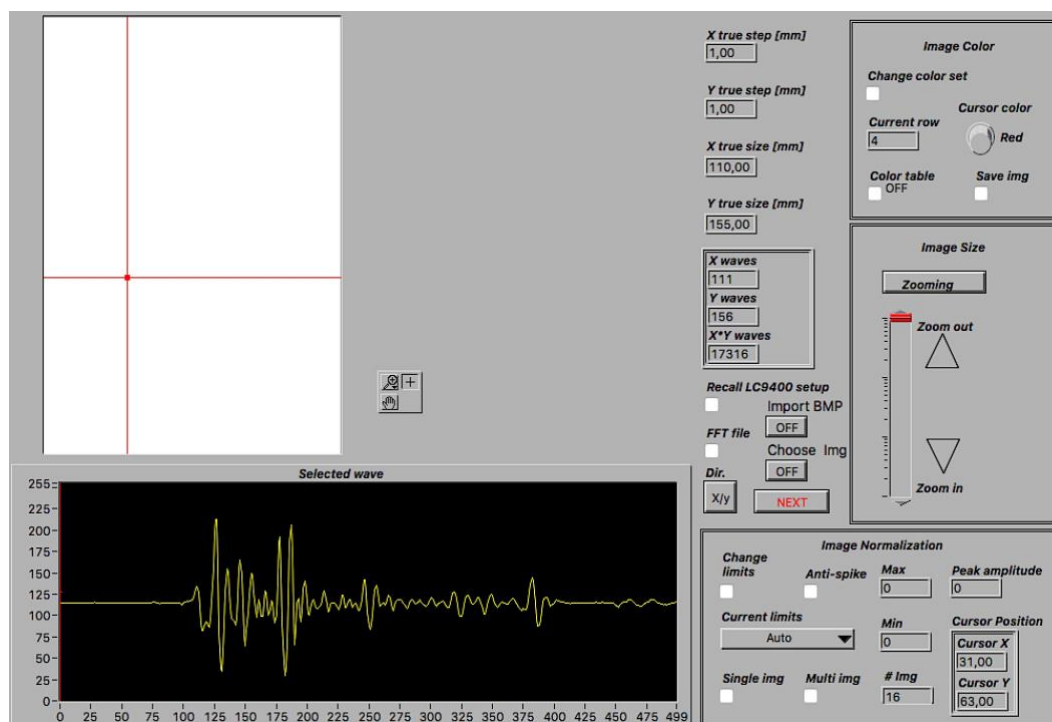


Figure 38. First Ecus Inspection© user interface with the 2D scheme of the scanned area of the QHL3IM1 laminate and the UT waveform relative to the scan point selected through the red cursor.



Figure 39. “Change Limits” user interface showing the selected complete UT waveform and its 16 time sub-gates (in the red rectangle).

The UT waveform enters the NCF laminate after travelling in water and, thus, the initial four images in the top row of Figure 40 were generated by the UT echoes reflected by stacking sequence $[+45^\circ/0^\circ/-45^\circ/90^\circ, +45^\circ/0^\circ/-45^\circ/90^\circ]$ in the first 1 mm thickness portion. Stacking sequence $[90^\circ/-45^\circ/0^\circ/+45^\circ, 90^\circ/-45^\circ/0^\circ/+45^\circ]$ characterizes the second row of four images in Figure 40, corresponding to the second 1 mm thickness portion. Due to the symmetrical structure of the NCF laminate, the stacking sequence of the third 1 mm thickness portions is $[+45^\circ/0^\circ/-45^\circ/90^\circ, +45^\circ/0^\circ/-45^\circ/90^\circ]$ (third row of four images in Figure 40) and the stacking sequence of the fourth 1 mm thickness portion is $[90^\circ/-45^\circ/0^\circ/+45^\circ, 90^\circ/-45^\circ/0^\circ/+45^\circ]$ (fourth row of four images in Figure 40)

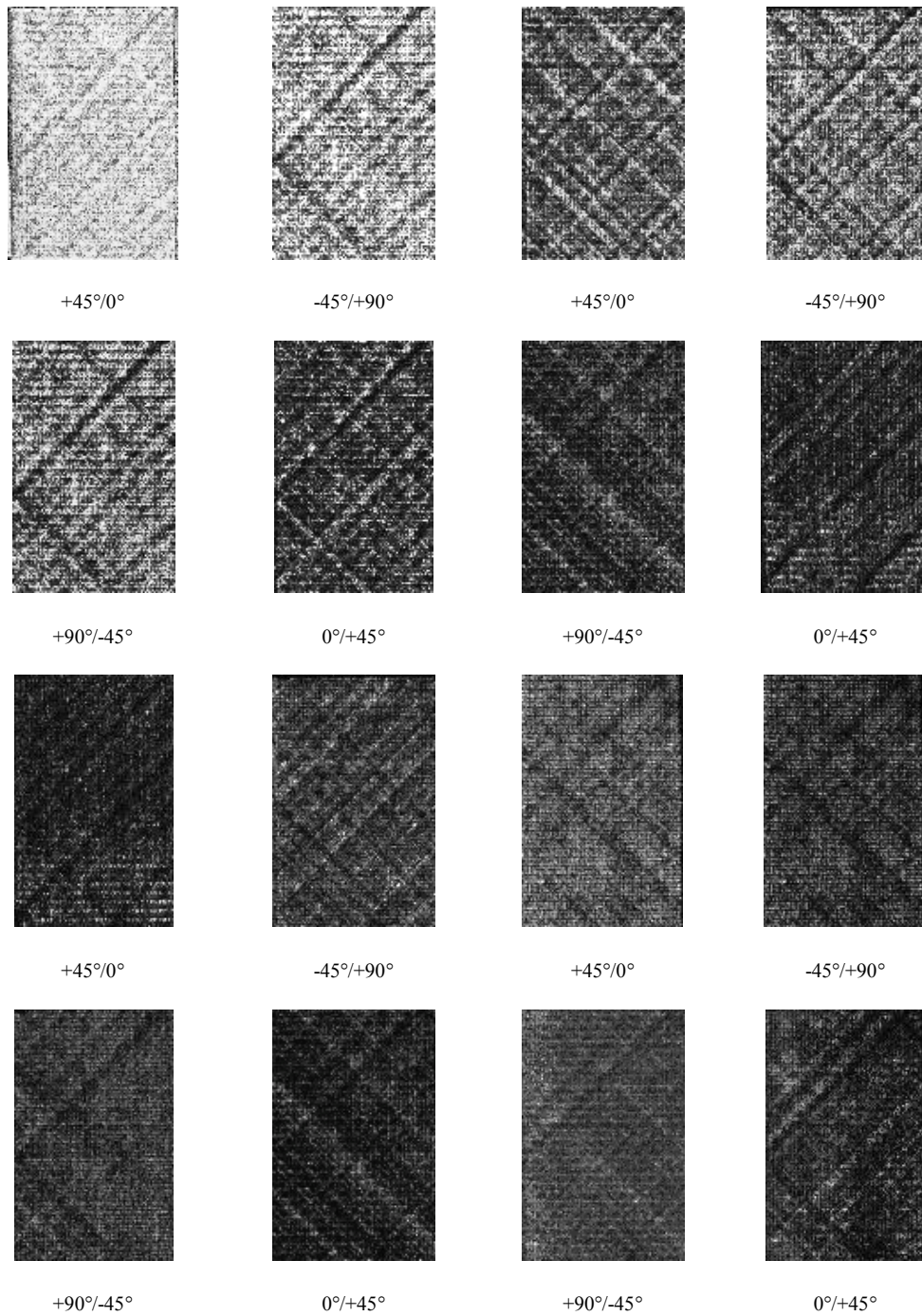


Figure 40. Sixteen UT images of the not impacted quadriaxial laminate QHL3IM1. Each UT image, arranged in succession from left to right and from top to bottom, relates to 1/16th of the laminate nominal thickness comprising two diverse consecutive fiber orientations in the stacking sequence [+45°/0°/-45°/90°, +45°/0°/-45°/90°, 90°/-45°/0°/+45°, 90°/-45°/0°/+45°]s.

4.2.4.2 Thickness calculation

The second objective of the metrological characterization is to verify if the total laminate and the single layer thicknesses correspond to the nominal ones. The actual thickness, s , of the not impacted NCF composite specimen QHL3IM1 was estimated through formula:

$$v = \frac{s}{(dt/2)}$$

where v is the UT velocity in the NCF composite and dt is the time of flight (ToF), i.e. the time it takes the UT signal to traverse to and fro the complete NCF composite laminate thickness. Therefore, in order to calculate the total thickness the time gate was set on the whole UT signal (Figure 41), in particular on the Frontal echo (relative to the beginning of the laminate) and on the Back echo (relative to the end of laminate). The total time distance measured, through the software Ecus Inspection©, between the Frontal and the Back echo is $dt = 2.665 \mu\text{s}$. By selecting an average UT velocity in the NCF composite equal to 3000 m/s, the thickness of the NCF specimen calculated by the previous formula is $s = 3.98 \text{ mm}$, which is very close to the nominal thickness of 4 mm.

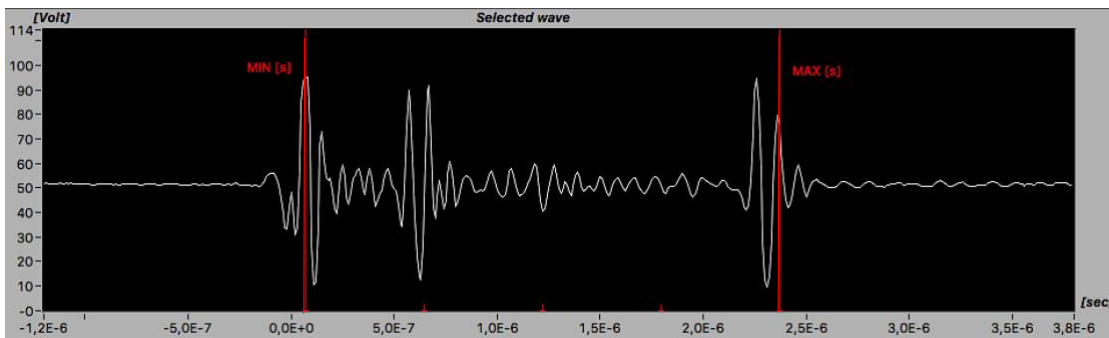


Figure 41. Time gate set on the Frontal and Back echoes of the QHL3IM1 laminate UT waveform.

In order to calculate the thicknesses of each layers, the dt to be substituted in the previous formula corresponds to the ToF of each time sub-gates. The calculated thicknesses are reported in the Table 3, these values highlight their correspondence to the nominal value equal to 0.25 mm. The small difference of $\pm 0.01 \text{ mm}$ can be attributed to minor variations of the

local UT velocity with respect to the selected value of 3000 m/s that represents the average UT velocity in the whole composite volume.

Stacking sequence	ToF min [s]	ToF max [s]	ΔT [s]	UT velocity [m/s]	Thickness [mm]
+45°/0°	1.63E-08	1.80E-07	1.64E-07	3000	0.25
-45°/90°	1.80E-07	3.43E-07	1.63E-07	3000	0.24
+45°/0°	3.43E-07	5.07E-07	1.64E-07	3000	0.25
-45°/90°	5.07E-07	6.76E-07	1.69E-07	3000	0.25
90°/-45°	6.76E-07	8.45E-07	1.69E-07	3000	0.25
0°/+45°	8.45E-07	1.01E-06	1.65E-07	3000	0.25
90°/-45°	1.01E-06	1.18E-06	1.70E-07	3000	0.26
0°/+45°	1.18E-06	1.34E-06	1.60E-07	3000	0.24
+45°/0°	1.34E-06	1.50E-06	1.60E-07	3000	0.24
-45°/90°	1.50E-06	1.67E-06	1.70E-07	3000	0.26
+45°/0°	1.67E-06	1.84E-06	1.70E-07	3000	0.26
-45°/90°	1.84E-06	2.01E-06	1.70E-07	3000	0.26
90°/-45°	2.01E-06	2.18E-06	1.70E-07	3000	0.26
0°/+45°	2.18E-06	2.34E-06	1.60E-07	3000	0.24
90°/-45°	2.34E-06	2.51E-06	1.70E-07	3000	0.26
0°/+45°	2.51E-06	2.67E-06	1.60E-07	3000	0.24
NCF total thickness	1.07E-08	2.66E-06	2.67E-06	3000	3.98

Table 3. Results for NCF composite thickness portions comprising two diverse consecutive fiber orientations in the laminate stacking sequence.

4.2.5 Quality assessment of the CFRP NCF laminates

As introduced in paragraph 4.1 Introduction, the quality assessment of the seven CFRP NCF laminates subjected to impact tests (with different impact energy) was carried out by:

- analysing the damage transition in the laminate stacking sequence
- calculating the damage position in the thickness direction (see Table 2).

4.2.5.1 Damage transition in the stacking sequence

The analysis of the damage transition in the stacking sequence was performed through the visual examination of the UT images relative to the internal structure of the seven CFRP NCF impacted laminates. In this thesis work, the results obtained for three (QHL3IM2, QHL3IM5 and QHL3IM8) of the seven laminates corresponding to low, medium and high impact energy (9 J, 20 J and 40 J) are reported. In order to perform the analysis, 4 UT images were generated for each of the three laminates, setting the time gate on the whole UT signal (Frontal and Back echoes) and dividing it in 4 equals time sub-gates (Figure 42). Repeating (only for greater clarity) what explained in the paragraph 3.4.2 Ecus Inspection© – UT images generation “as the time axis orientation corresponds to the UT waveforms propagation in the sample thickness direction, the time sub-gate width identifies the thickness portion to be imaged, therefore each UT image corresponds to the internal structure of the sample thickness portion identified by the relative time sub-gate”) it is clear that the 4 generated UT images correspond to 1/4 of the laminate thickness ($4 \text{ mm} / 4 \text{ sub-gates} = 1 \text{ mm}/\text{image}$).

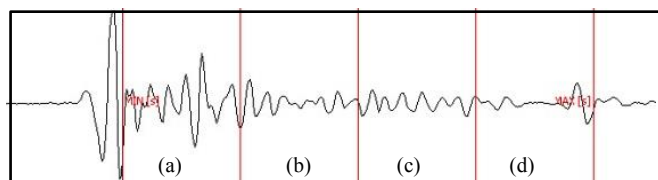


Figure 42. Time gate divided into 4 time sub-gates.

By examining the UT images in the Figure 43, 44 and 45, it can be noted that the impact damage develops differently at interfaces between layers with diverse fiber orientations.

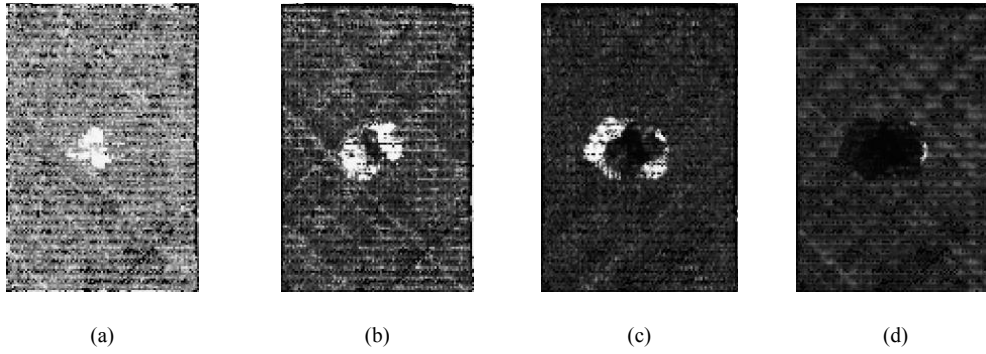


Figure 43. 4 UT images for low energy (9 J) impacted NCF laminate specimen QHL3IM2: (a) surface damage, (b) and (c) internal damage, (d) in-plane projection of the total damage.

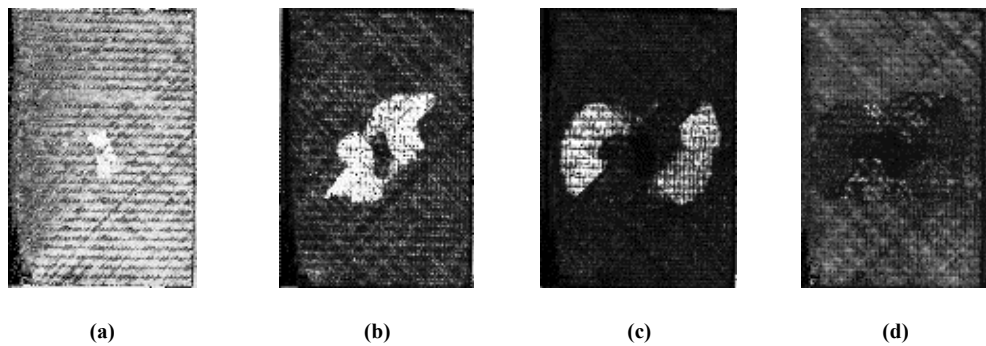


Figure 44. 4 UT images for medium energy (20 J) impacted NCF laminate specimen QHL3IM5: (a) surface damage, (b) and (c) internal damage, (d) in-plane projection of the total damage.

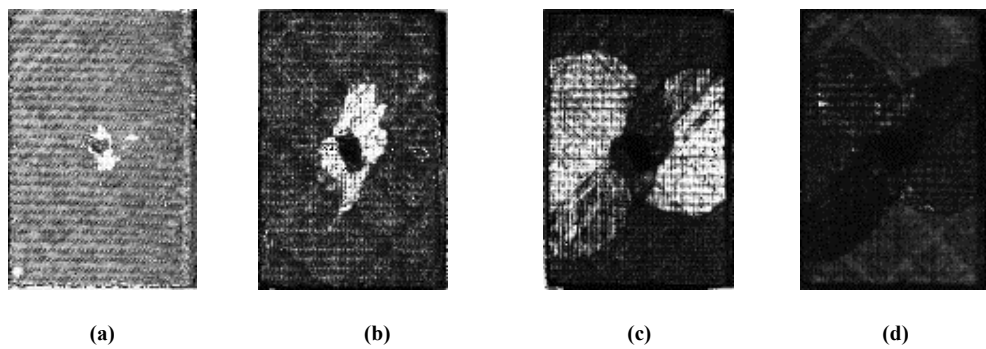


Figure 45. Four UT images for high energy (40 J) impacted NCF laminate specimen QHL3IM8: (a) surface damage, (b) and (c) internal damage, (d) in-plane projection of the total damage.

Moreover, the delamination extension increases with rising distance (depth) from the impact surface and with growing impact energy known as hat-shaped configuration of the delamination. The UT analysis also reveals the absence of delamination in the zone directly below the impact surface contact point.

The Figure 41 (d), 42 (d) and 43 (d) display UT images that stand for the in-plane projection of the damage developed at different depths in the whole laminate thickness, rather than just the damage in the fourth (lowest) 1 mm thickness portion. Their examination allows to assess the overall damage in the material according to the conventional UT C-scan technique and can be used for total delaminated area measurement.

4.2.5.2 Damage position in the thickness direction

The damage position in the thickness direction is evaluated by analysing 16 UT images generated for each impacted NCF laminate according to the procedure described in the paragraph 4.2.4.2 Thickness calculation, i.e.:

- 1) performing the UT FV pulse-echo immersion scanning
- 2) processing the resulting UT volumetric data file with Ecus Inspection© in order to obtain multiple UT images of the internal structure of the inspected laminate
- 3) analysing the results in order to identify where the damage occurs
- 4) utilising the time of flight (relative to the damage time sub-gate) to calculate the thickness (i.e. the depth of damage)

In particular for each laminate, 16 UT images (Figure 46) were generated setting the time gate on the whole UT signal and dividing it into 16 equal time sub-gates.

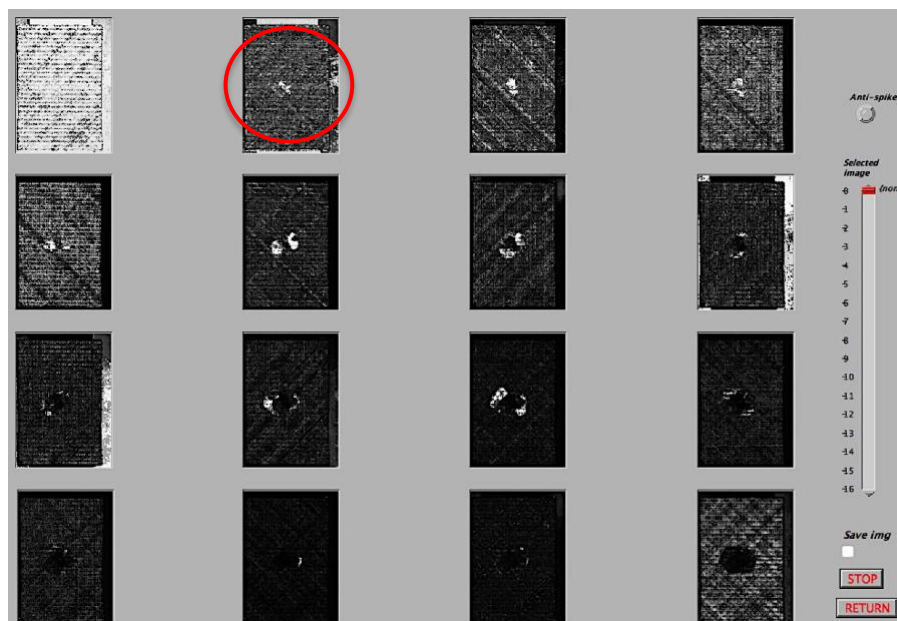


Figure 46. 16 UT images of the QHL3IM impacted laminate.

After identifying the image containing the damage and the corresponding laminate thickness portion, the damage position in the thickness direction was evaluated by substituting the ToF value related to the time gate for that thickness portion in the formula.

In particular, the circled image in Figure 46 represents the first UT image in which the damage appears, therefore its time of flight is used to calculate the relative thickness (depth).

In Table 4 the damage position is reported for each impacted specimen in terms of start of damage, start of delamination and maximum delamination extension, evaluated from the frontal surface in the thickness direction.

Samples ID	Damage position [mm]	Delamination position [mm]	Delamination maximum extension position [mm]
QHL3IM2	0.3110	1.1245	2.615
QHL3IM3	0.0124	1.1245	2.810
QHL3IM4	0.1876	1.1260	2.555
QHL3IM5	0.0615	1.1250	2.435
QHL3IM6	0.2498	1.1245	2.750
QHL3IM7	0.0623	1.0615	2.510
QHL3IM8	0.0062	1.1875	2.690

Table 4. Damage position direction, delamination position and maximum delamination area extension position in the thickness direction for each impacted sample.

It can be noted that:

- damage occurs near the upper surface, except for specimens 2, 4 and 6 for which the depth is slightly larger
- delamination is manifested for all laminates at about 1.1 mm in depth
- delamination maximum extension is between 2.4 and 2.6 mm in depth, except for the 3, 6 and 8 specimens for which the depth is greater

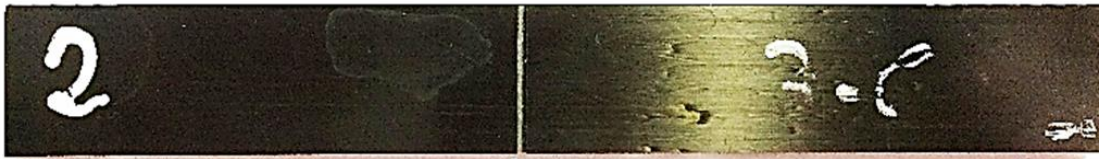
Results show that the impact damage development was effectively well characterized by evaluating the damage position in the laminate thickness direction and by identifying the different damage shapes at interfaces between layers with diverse fiber orientations in the stacking sequence.

4.3 Case Study n° 2 - Quality assessment of the adhesive bonding process for CFRP laminates

Adhesive bonding process is an optimal junction technique for the CFRP composites since it does not require any machining process (that reduce the structural material integrity) and it adds a very small weight to the composite structure [40]. The adhesive joints mechanical properties depends on several parameters including width, depth and continuity of the applied adhesive layer [41, 42] but the main one is its homogeneity. Therefore, this second case study is focused on a quality assessment of the adhesive bonding process for CFRP laminates in terms of adhesive layer homogeneity (that corresponds to the adhesive thickness variation). After the UT FV scanning performed on the specimens under examination, the UT images of their internal structure were generated in order to obtain a 2.5D axial tomography. Finally, the quality assessment of the utilized bonding process was carried out through a custom-made software properly developed in Matlab® environment to provide a 3D thickness reconstruction of the defects by processing the UT volumetric scanning data.

4.3.1 CFRP adhesive bonded joint laminates material

CFRP components, manufactured by various processes, often are then subjected to joining processes, as that via adhesive, for an easy assembly of the light weight structures. In particular, for the CFRP laminates inspected in this second case study (Figure 47), a single lap adhesive joints were realized according to ASTM D 3165 [43], using an epoxy matrix carbon fiber reinforced plastic substrate and an EA9394 thixotropic adhesive with a nominal thickness of 0.254 mm and tolerance ± 0.051 mm (Figure 48). The adherents consist of 8 layers of unidirectional carbon fiber/epoxy (see also the relative UT images reported in Figure 53) with 0.25 mm thickness each, obtaining a laminate of nominal thickness 2.00 mm, and were produced in autoclave. The bonding surfaces were appropriately cleaned, dried and treated according to ASTM D 2093 [44]. After preparing the surfaces, a layer of the adhesive was applied. The parts were lined up by reference pins in a tool for bonding and then a pressure was applied. The utilized cure conditions were indicated by the manufacturer of the adhesive.



(a)



(b)

Figure 47. CFRP adhesive bonded joint: (a) Frontal and (b) side view.

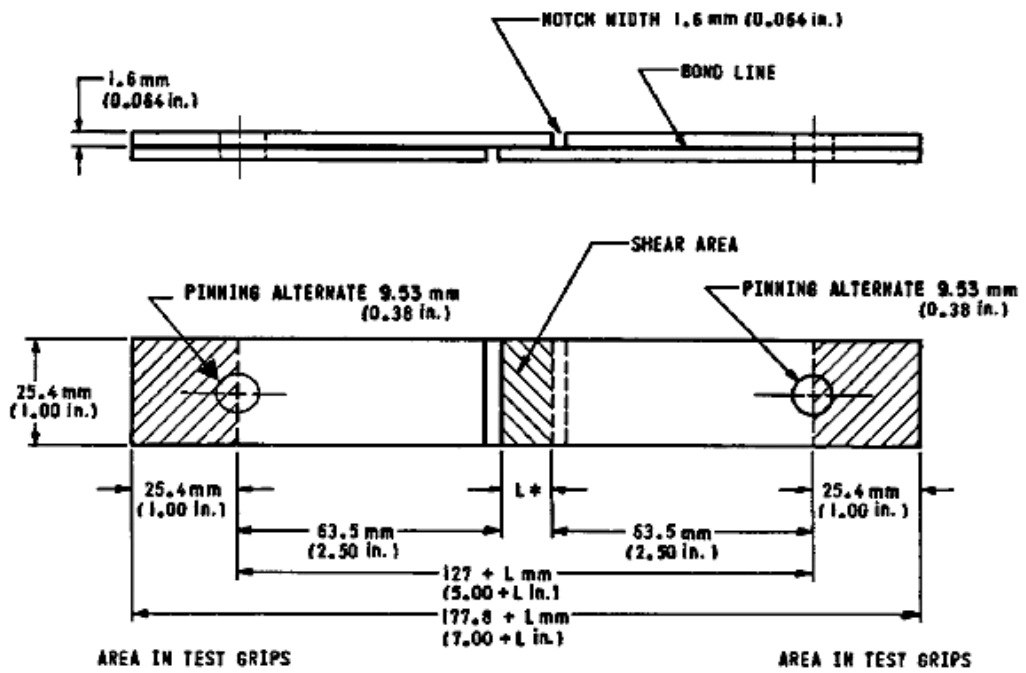


Figure 48. Form and dimension of Test Specimen [37].

4.3.2 Adhesive bonding process defects

As pre mentioned, the homogeneity of the adhesive layer is the main parameter that affects the mechanical properties of the adhesive bonded joint. The failure of the bonding process may take place due to an inadequate application of the adhesive layer. Moreover it can occur in different ways, such as cohesive fracture, interface fracture or mixed fracture and falling of the adhering, as shown in the Figure 49.

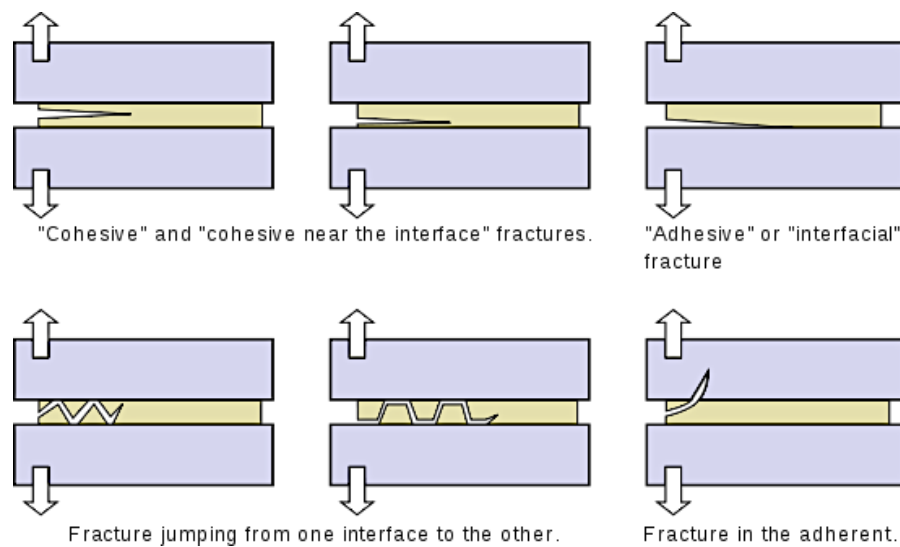


Figure 49. Different failure ways of the adhesive bonding joint.

4.3.3 UT FV scanning based on pulse-echo immersion testing of CFRP adhesive bonded joint laminates

The UT FV scanning based on pulse-echo immersion testing was executed on the CFRP adhesive bonded joint laminates (Figure 50) with the same settings listed in the paragraph 4.2.3 UT FV scanning based on pulse-echo immersion testing of CFRP NCF laminates except for the scanning area that, in this case, is equal to 15 (y direction) x 15 mm (xy direction) Figure 51. The y scan direction was selected to correspond to the bonded joint longitudinal axis, which is also the direction of the unidirectional fibers in the external laminates, and the x scan direction was orthogonal to the unidirectional fibers in the external laminates.

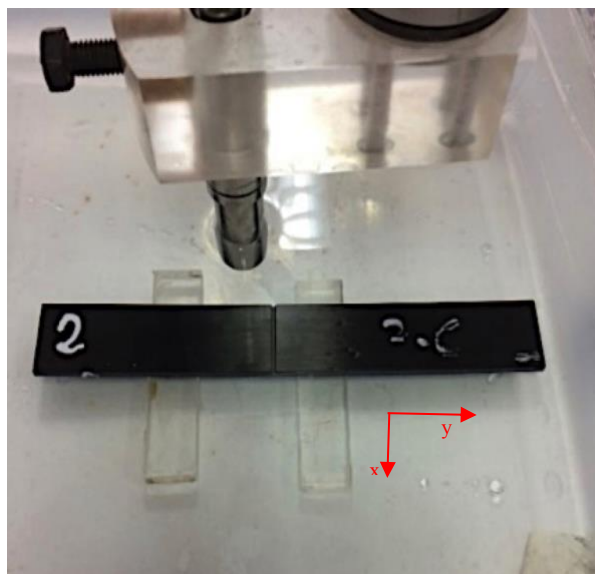


Figure 50. UT FV scan of the adhesive bonded joint laminate with the two scan directions x-y.

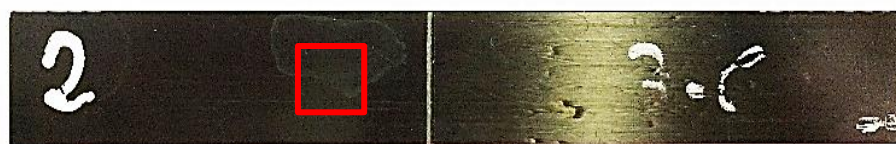


Figure 51. Adhesive bonding joint laminate scanned area of 15 x 15 mm (red square).

4.3.4 UT images generation of the CFRP adhesive bonded joint laminates

Performed the scanning, from the resulting UT volumetric file, single or multiple UT images of the internal structure of the CFRP component under examination can be obtained. To achieve the UT images, as widely illustrated in the previous paragraphs, a time gate needs to be set on a selected typical UT waveform (Figure 52) and divided into a number of equal time sub-gates for multiple images generation (also in this case 16 time sub-gates are set). Figure 53 shows the obtained 16 UT images corresponding to $1/16^{\text{th}}$ of each CFRP component nominal thickness. It can be observed that the CFRP adhesive bonded joint laminate consists of unidirectional reinforcement fiber bundles oriented at 0° with respect to the specimen axis and held together by transversal filaments. Moreover, the adhesive layer begins to appear together with the unidirectional fibers in the 7th UT image (first red circle in the Figure 53) and tends to disappear in the 10th UT image (second red circle in the Figure 53).

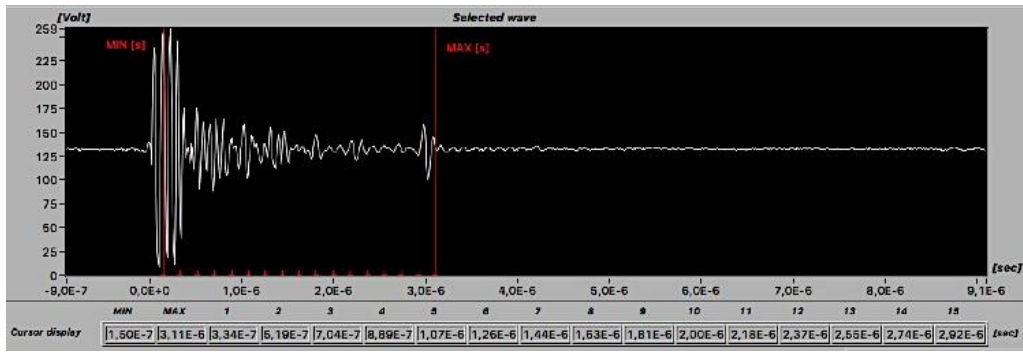


Figure 52. Typical UT waveform of the UT volumetric file for the CFRP adhesive bonded joint with the time gate divided in 16 time sub-gates.

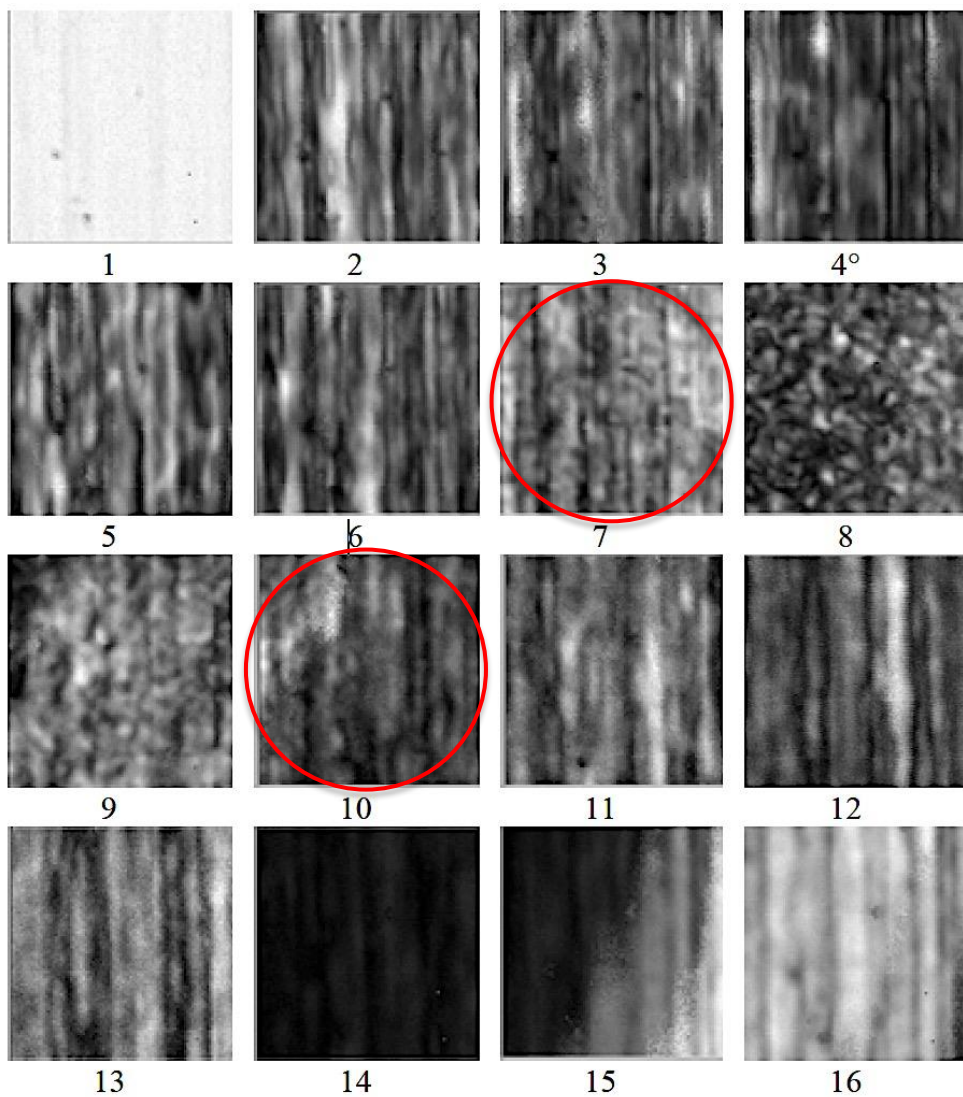
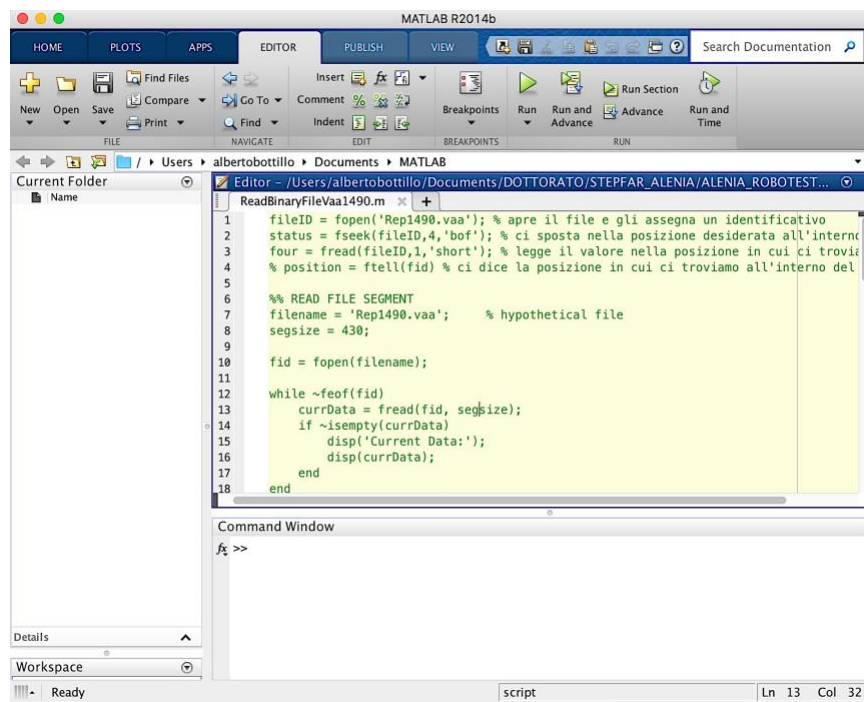


Figure 53. Sixteen UT images of the adhesive bonded joint laminate. Each UT image, arranged from left to right and from top to bottom, relates to 1/16 of the laminate nominal thickness.

4.3.5 Matlab® custom-made analysis software

The 3D thickness reconstruction of the CFRP adhesive bonded joint laminates was carried out using a custom-made software code properly developed in Matlab® environment (Figure 54) in order to evaluate the homogeneity of the internal adhesive layer. The functionalities of the software consist of:

- extraction of the UT waveforms from the acquired UT volumetric data file and their storage in *.txt file
- single UT waveform processing for the recognition of the relevant echoes
- thickness measurement
- 3D thickness representation



```
1 ReadBinaryFileVaa1490.m
2 fileId = fopen('Rep1490.vaa'); % apre il file e gli assegna un identificativo
3 status = fseek(fileID,4,'bof'); % ci sposta nella posizione desiderata all'interno
4 four = fread(fileID,1,'short'); % legge il valore nella posizione in cui ci trovia
5 % position = ftell(fid) % ci dice la posizione in cui ci troviamo all'interno del
6
7 %% READ FILE SEGMENT
8 filename = 'Rep1490.vaa'; % hypothetical file
9 segsize = 430;
10
11 fid = fopen(filename);
12
13 while ~feof(fid)
14     currData = fread(fid, segsize);
15     if ~isempty(currData)
16         disp('Current Data:');
17         disp(currData);
18     end
19 end
```

Figure 54. Firsts code line of the custom-made Matlab® software developed at the Fraunhofer Joint Laboratory of Excellence on Advanced Production Technology [39].

4.3.5.1 UT waveforms extracting and saving

The first steps executed by the custom-made software is to extract the UT complete waveforms from the UT volumetric data file and to save them into x,y.txt file where x and y represent the scan points coordinate (following the boustrophedonic raster path).

4.3.5.2 Relevant echoes identification

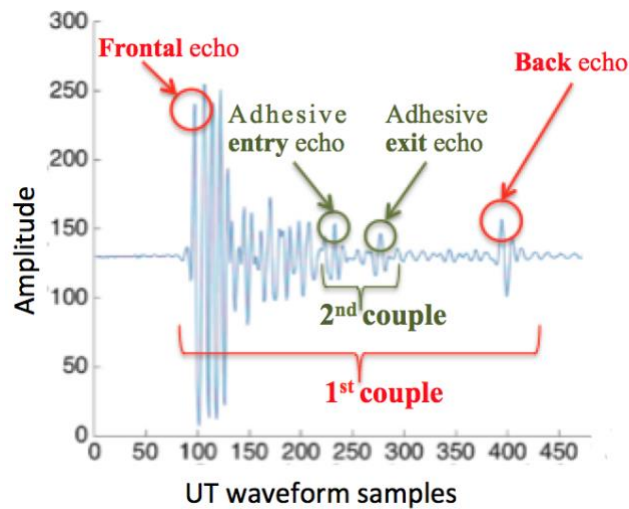
Extracted and saved the UT waveforms in .txt file, the software process them in order to recognise the relevant echoes. When the software is launched, a pop-up opens asking to indicate:

- the number of equal portions in which divide the UT waveforms (each portion is indicated by a letter, according to the alphabet letters order)
- the letters relative to two of the divided portions in which the software will recognise the maximum peak (e.g. putting A - C the software understand that it has to recognise the maximum peak in the first (A) and in the third (C) waveform portion)

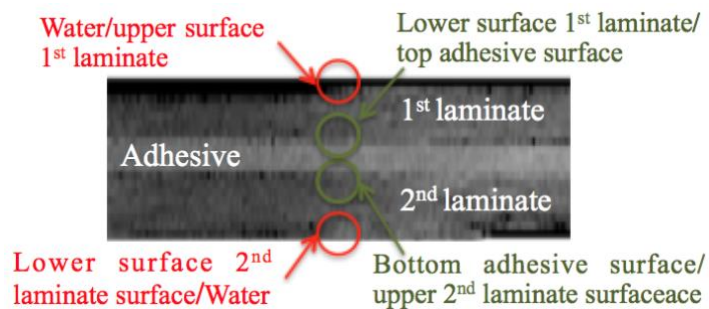
These inputs obviously have to be provided to the software after an accurate visual analysis of the complete UT waveform and of the relative UT images (see paragraph 4.3.4 UT images generation of the CFRP adhesive bonded joint laminates) and depending on the goal of the examination. As the objective is to evaluate the adhesive layer homogeneity (corresponding to its thickness variation) the relevant echoes to be identify are the ones relative to the entry and the exit of the UT waveforms. Furthermore, having to evaluate also the thickness of the whole bonded laminates, the relevant echoes corresponding to the beginning and the end of the laminate thick have to be identified too.

In Figure 55 a generic complete UT waveform of the CFRP adhesive bonded joint laminates (a) and their side view (b) are reported. In particular, the two couple of relevant echoes highlighted by the red circles are the followings:

- 1) the first couple is constituted by the Frontal echo (first circle on the left) representing the interface between the water and the upper surface of the first CFRP laminate (adherend), and the Back Echo (last circle on the right) that represents the interface between the lower surface of the second CFRP laminate (adherend) and the water
- 2) the second couple is constituted by the two middle circled echoes representing (from left to the right) the interface between the lower surface of the first CFRP laminate (adherend) and the adhesive layer top surface, and between the bottom surface of the adhesive layer and the upper surface of the second CFRP laminate (adherend)



(a)



(b)

Figure 55. (a) Generic UT waveform of the CFRP adhesive bonded joint laminates with the two couples of relevant echoes: the 1st composed by the Frontal and the Back echoes, the 2nd one by the middle echoes; (b) laminate side view with the interfaces corresponding to the relevant echoes.

4.3.5.3 Thickness calculation

In order to calculate the thicknesses (s) the software converts the distance between the relevant echoes, expressed in number of samples, into temporal distance (ToF) which represents the time necessary for the UT signal for traversing to and fro the thickness portion identified by the two selected relevant echoes and then substitutes it with dt in the simple formula:

$$v = \frac{s}{(dt/2)}$$

In particular the distance between the relevant echoes of the first couple corresponds to the thickness of the whole bonded laminates, while the distance between the echoes of the second one corresponds to the thickness of the adhesive layer. In Figure 56 is reported a generic complete UT waveform of the CFRP adhesive bonded joint laminate showing these correspondences.

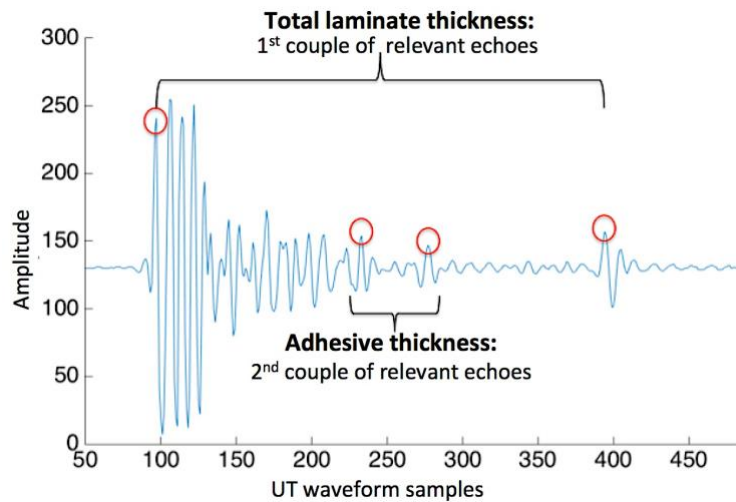
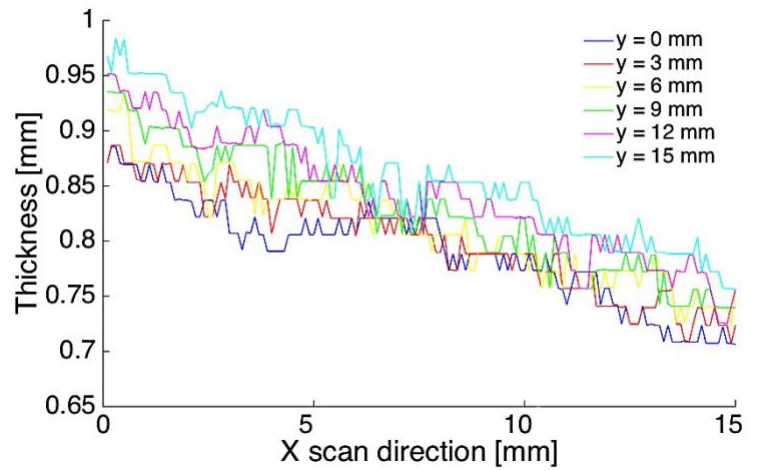


Figure 56. Generic UT waveform of the CFRP adhesive bonded joint laminates with the correspondence to the thickness portions they represent.

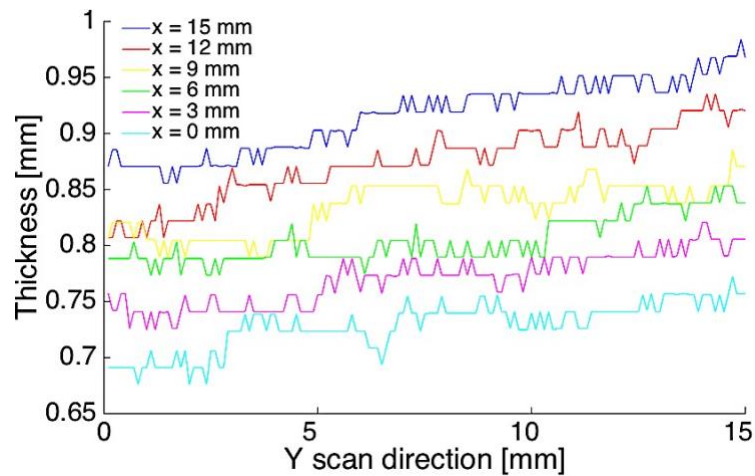
4.3.5.4 3D thickness reconstruction for the quality assessment of the bonding process

The last functionality executed from the custom-made software is to represent the calculated thicknesses both in a two axis graphs and in a 3D view in order to assess the quality of the bonding process. In

Figure 57 the curves of the adhesive thickness as a function of the x and y scan directions are reported. In particular for the Figure 57 (a) each coloured curve represents the adhesive thickness measured along the x direction at a specific y value ($y = 0, 3, 6, 9, 12, 15$ mm). Similarly, in Figure 57 (b), the measured adhesive thicknesses along the y scan direction are reported for a specific x value ($x = 0, 3, 6, 9, 12, 15$ mm).



(a)



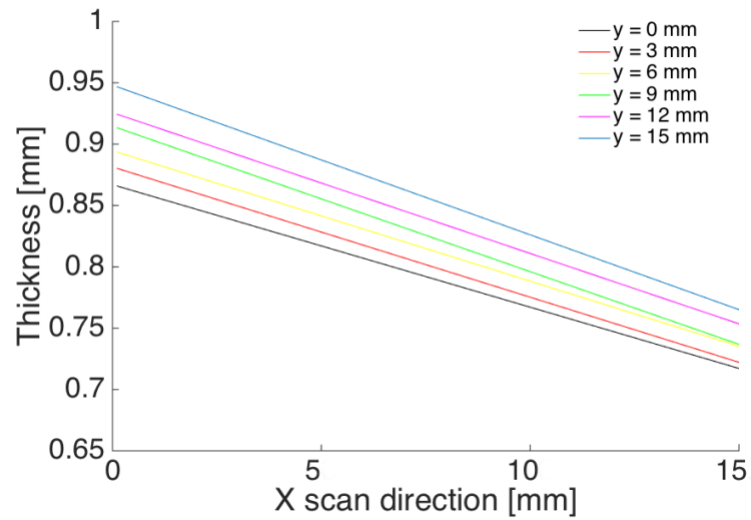
(b)

Figure 57. Adhesive thicknesses measured (a) along the x direction at $y = 0, 3, 6, 9, 12, 15$ mm and similarly (b) along the y direction at $x = 0, 3, 6, 9, 12, 15$ mm).

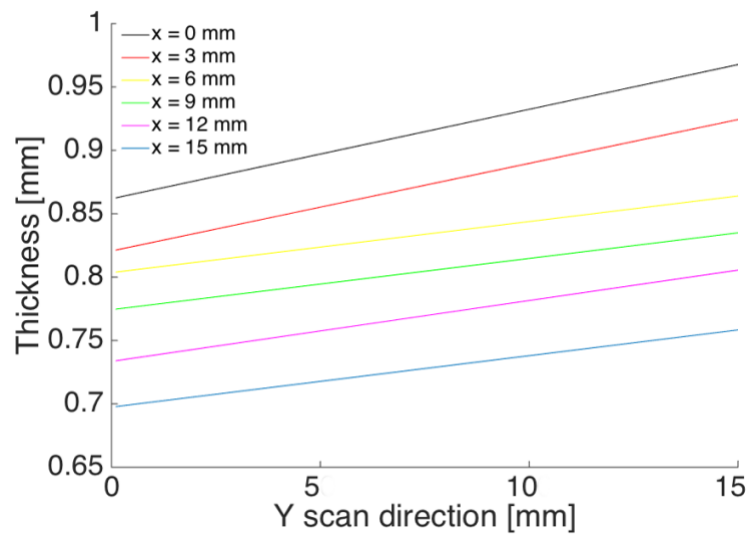
In the Figure 58 are reported the interpolations of the previous curves in which is more evident the result of

Figure 57, i.e. that the thickness of the internal adhesive layer is not constant along the two x-y directions of the scan. Indeed, Figure 58 (a) shows that the thickness of the adhesive layer decreases along the x scan direction for each y value. Specifically, for $y = 0, 3, 6, 9, 12, 15$ mm the measured thickness ranges are respectively: 0.870 - 0.691, 0.871 - 0.724, 0.919 - 0.724, 0.935 - 0.741, 0.953 - 0.741, 0.968 - 0.757 mm. Moreover, the curves slope rises with increasing y value, ranging between -14.5° and -17.8° .

In Figure 58 (b), the thickness of the adhesive layer increases along the y scan direction for each x value. In particular, for x = 0, 3, 6, 9, 12, 15 mm the measured thickness ranges are respectively: 0.871 - 0.968, 0.807 - 0.920, 0.806 - 0.871, 0.788 - 0.803, 0.757 - 0.806, 0.691 - 0.757 mm. Furthermore, the curves slope generally increases with increasing x value, ranging between 5.8° and 12.3°.



(a)

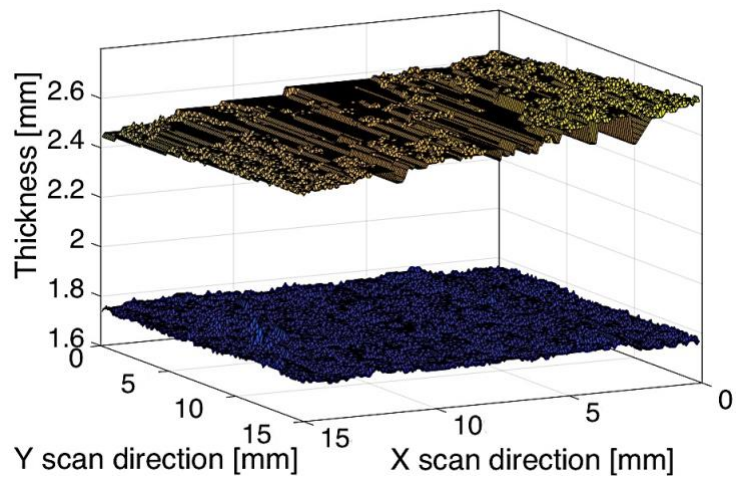


(b)

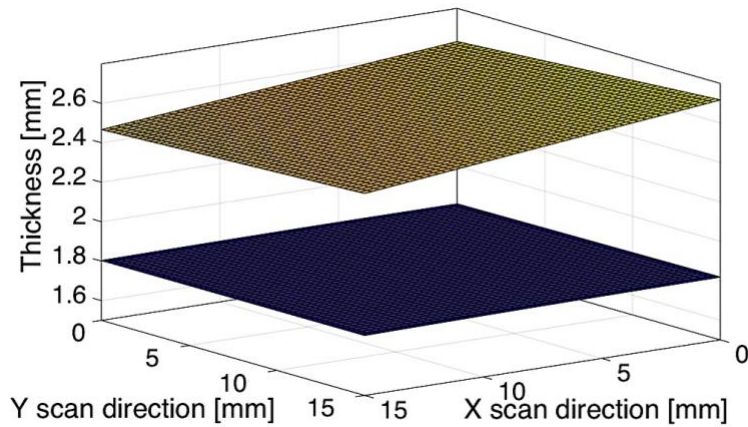
Figure 58. Interpolated curves of the adhesive thicknesses measured along (a) the x and (b) y direction of scan.

In Figure 59 (a), a 3D representation of the top (entry) and bottom (exit) adhesive/adherent interfaces is reported highlighting the adhesive thickness double slope variation in both the x

and y scan directions. In Figure 59 (b) the interfaces interpolation is reported too. This thickness variation influences the total thickness of the CFRP sample. Accordingly, the total thickness of the entire CFRP sample (two external laminates plus adhesive layer) was measured considering the Frontal and the Back echoes of the characteristic UT waveform of the volumetric UT file.



(a)

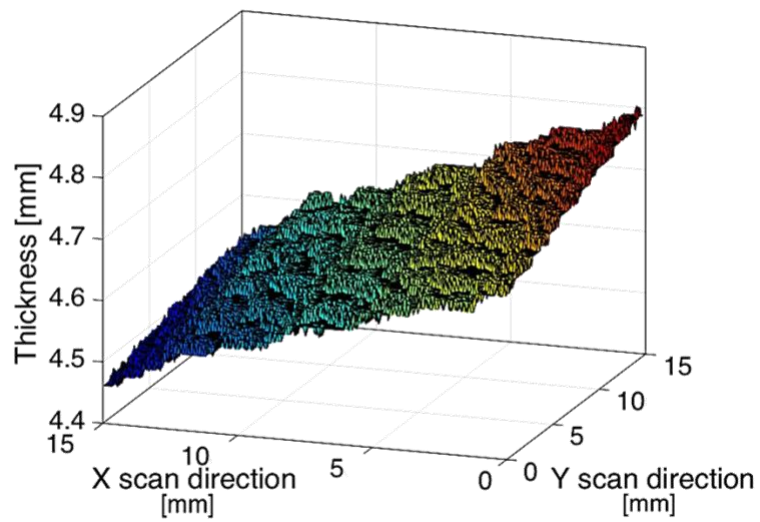


(b)

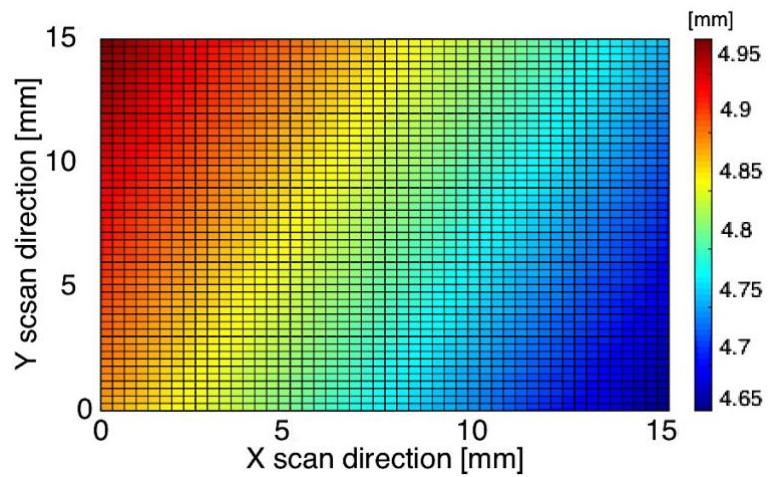
Figure 59. Adhesive (a) top (yellow) and bottom (blue) surfaces and (b) their fitting.

In Figure 60 (a) and (b) the total thickness of the entire CFRP sample is represented as a colour map where the false colours indicate the total thickness values. The colour fringes, corresponding to constant thickness in the colour map, display an orientation of about 28° with respect to the y scan direction which corresponds to the direction of the unidirectional

fibers in the external laminates. This confirms the presence of a double slope of the top sample surface with higher slope value in the x scan direction and lower slope value in the y scan direction. The total CFRP sample thickness varies between 4.957 and 4.617 mm.



(a)



(b)

Figure 60. Colour map of the total thickness variation of the entire CFRP sample (two external laminates plus adhesive layer): (a) 3D view, (b) top view.

4.4 Case Study n° 3 - Quality assessment of the drilling process for CFRP laminates

This third and last case study is focused on a quality assessment of the drilling process for CFRP drilled laminates in terms of presence of the push-out delamination (also known in industrial field as “Volcano effect”). As for the second case study, after performing the UT FV scanning based on pulse-echo immersion testing on the examined laminate, the UT images of its internal structure are generated in order to obtain a 2.5D axial tomography. Then the quality assessment of the drilling process is carried out elaborating the UT volumetric data file (resulting from the UT FV scanning) by the Matlab® custom-made software (which functionalities were illustrated in the paragraph 4.3.5 Matlab® custom-made analysis software) so as to obtain the 3D thickness reconstruction of the drilled area to evaluate the presence of the Volcano effect.

4.4.1 CFRP drilled laminates material

The drilled CFRP laminates under inspection (Figure 61. CFRP drilled laminate) have a thickness of 5 mm and consist of 26 unidirectional prepreg plies (carbon fibers – Toray T300 and epoxy matrix – CYCOM 977-2) arranged according to $[\pm 45^{\circ}_2/0^{\circ}/90^{\circ}_4/0^{\circ}/90^{\circ}/0^{\circ}_2]_s$ stacking sequence. On the laminates top and bottom there is a very thin fiberglass/epoxy ply, reinforced with $0^{\circ}/90^{\circ}$ fabric which areal weight is 80 g/m^2 [41]. The laminates were produced by hand layup, vacuum moulding and subjected to an autoclave treatment process with the following parameters: temperature $180 \text{ }^{\circ}\text{C}$, pressure 6 bar and time: 180 min [45]. Therefore, to reproduce the stack drilling process performed in the aeronautic industry (for subsequent mechanical joining through riveting) drilling tests were performed on a stack made of two CFRP laminates [4]. In fact, in the aeronautical field the CFRP laminates are first superimposed and then drilled together. The utilized drill is a tungsten carbide twist drill with two flutes, 6.35 mm diameter, 125° point angle and 30° helix angle was employed. The following drilling parameters were set: rotational speed = 7500 rpm and feed = 0.2 mm/rev.



Figure 61. CFRP drilled laminate.

4.4.2 Drilling process defects

Drilling process is one of the most utilized in the aeronautic industry in order to produce holes for subsequent mechanical joints with screws and bolts (Figure 62). This process is often applied to composite materials even if it can present the inconvenient problem of the delamination which reduces the material structural integrity resulting in poor assembly tolerance [46, 47].



Figure 62. CFRP laminates mechanical joints through screws and bolts.

Delamination may occur around the drilled hole at both top and the bottom laminate surface, corresponding to the drill entry and exit (Figure 63). In particular, if the delamination appears around the drill entry area it is defined peel-up delamination, while if it occurs around the drill exit one it is named push-out delamination or Volcano effect. The hole exit (or push-out) delamination is generally more severe than the hole entry (or peel-up) delamination and tends to notably increase with tool wear [48].

About the push-out phenomenon, also known in the industry as “Volcano effect”, the laminate under the drill bit tends to be dragged away from the interlaminar bond around the hole due to the compressive thrust force (F_z in Fig. 63) applied by the drill bit. Near the end of the hole creation, the uncut thickness and the resistance to deformation decrease until the loading exceeds the interlaminar bond strength and delamination occurs.

These types of defects can be effectively investigated by employing UT NDE methods able to characterize delamination defects in terms of extent, shape and location within the laminate, and to measure the laminate thickness to evaluate the height of the peel-up and push-out effect around the holes.

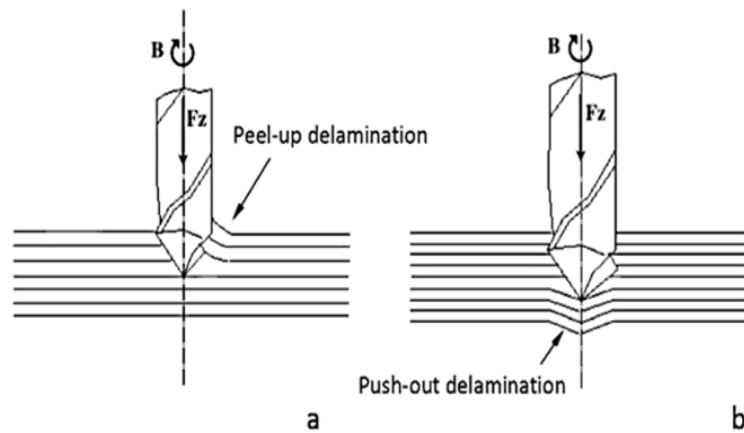


Figure 63. (a) Peel-up and (b) push-out delamination.

4.4.3 UT FV scanning based on pulse-echo immersion testing of CFRP Drilled laminates

The UT FV scanning based on pulse-echo immersion testing was executed on the CFRP Drilled laminate (Figure 64) with the same settings listed in the paragraph 4.2.3 UT FV scanning based on pulse-echo immersion testing of CFRP NCF laminates except for the scanning area (Figure 65) that is 14 (y direction) x 14 mm (x direction) [5]. The y scan direction was selected to correspond to the drilled sample longitudinal axis as well as to the 0° fiber direction in the quasi isotropic laminate, and the x scan direction corresponded to the 90° fiber direction in the quasi isotropic laminate.



Figure 64. Pulse-echo UT FV immersion scanning on the CFRP drilled laminates with the two scan directions x-y.

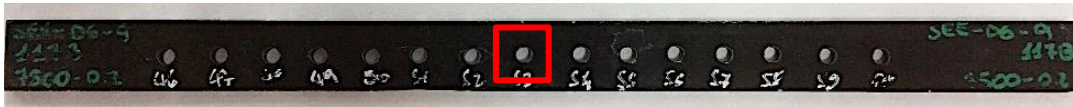


Figure 65. CFRP Drilled laminates with the scanning area of 14 x 14 mm (red square).

4.4.4 UT images generation of CFRP Drilled laminates

Also for this last case study, the UT volumetric data file was processed by Ecus Inspection© to generate multiple UT images. Setting the time gate on the UT signal and dividing it into 16 time sub-gates the software generates the 16 UT images reported in Figure 66. By observing the UT images it is possible to recognize the stacking sequence of the quasi-isotropic laminate sample $[\pm 45^{\circ}_2/0^{\circ}/90^{\circ}_4/0^{\circ}/90^{\circ}/0^{\circ}_2]_s$. Moreover, a Volcano effect is highlighted in the first UT image with fibers oriented at -45° . Finally, the shape of the hole (see in particular the 7th image) is significantly different from the nominal hole size, which indicates the presence of a delaminated area around the hole.

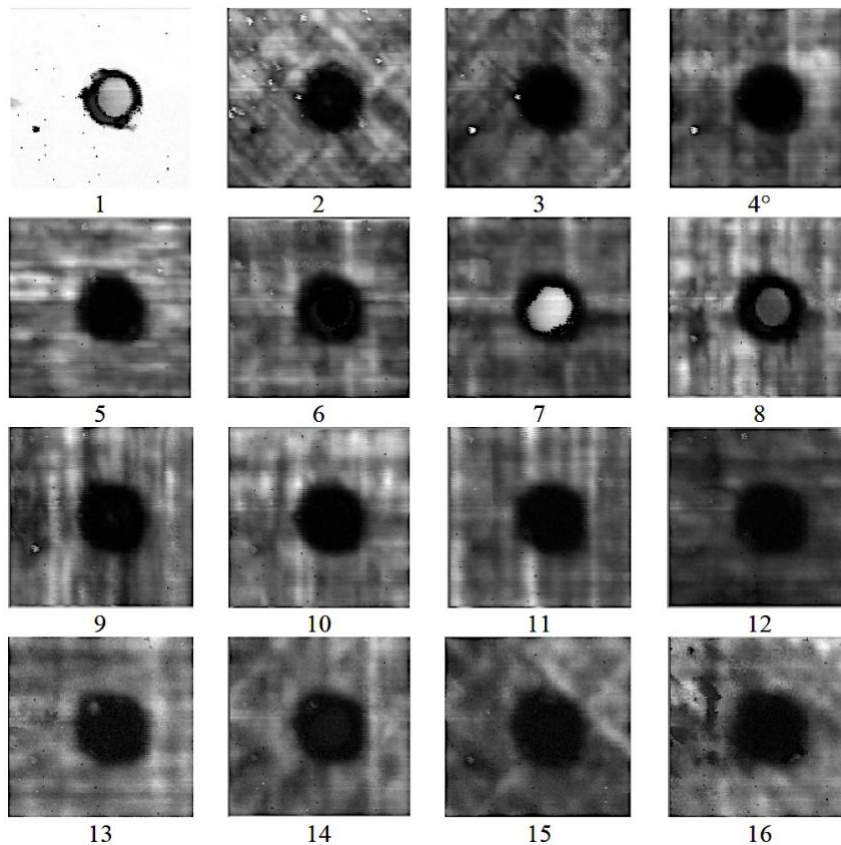


Figure 66. Sixteen UT images of the CFRP drilled laminate. Each UT image, arranged from left to right and from top to bottom, relates to 1/16 of the laminate nominal thickness.

4.4.5 Matlab® custom-made Analysis Software

The 3D thickness reconstruction of the CFRP drilled laminates is carried out using the Matlab® custom-made software illustrated in the paragraph 4.3.5 Matlab® custom-made analysis software hence its functionalities will be not repeated.

4.4.5.1 UT waveforms extracting and saving

The first steps executed by the custom-made software is to extract the UT complete waveforms from the UT volumetric data file and to save each of them into *.txt file (see paragraph 4.3.5.1 UT waveforms extracting and saving

4.4.5.2 Relevant echoes identification

Analogously to what seen for the second case study in the paragraph 4.3.5.2 Relevant echoes identification in Figure 67 is reported a generic complete UT waveform of the drilled laminate under inspection. As in this third case it has to verify the presence of the Volcano effect, that influences the total laminate thickness (corresponding to a displacement of the Back echo on the time axis), the relevant echoes must be recognised are the Frontal and the Back ones (which represent the beginning and the end of the laminate respectively).

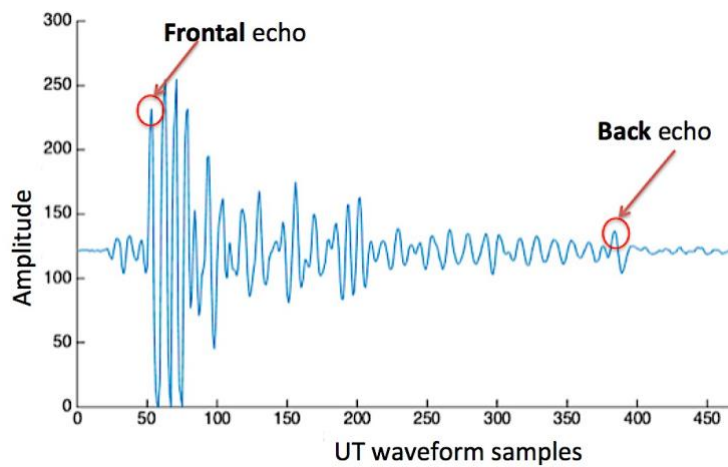


Figure 67. Generic UT waveform of the CFRP drilled laminate with one couple of relevant echoes: the Frontal and the Back echoes.

4.4.5.3 Thickness calculation

Once the relevant echoes were recognised, the software to calculate the thicknesses (s) converts the distance between each of them, expressed in number of samples, into temporal distance (ToF) which represents the time taken by the UT signal for traversing to and fro the thickness portion identified by the two selected relevant echoes and then substitutes it with dt in the simple and already known formula:

$$v = \frac{s}{(dt/2)}$$

In Figure 68 is reported a generic complete UT waveform of the CFRP drilled laminate with the correspondence between the couple of relevant echoes distance and the thickness portion they represent.

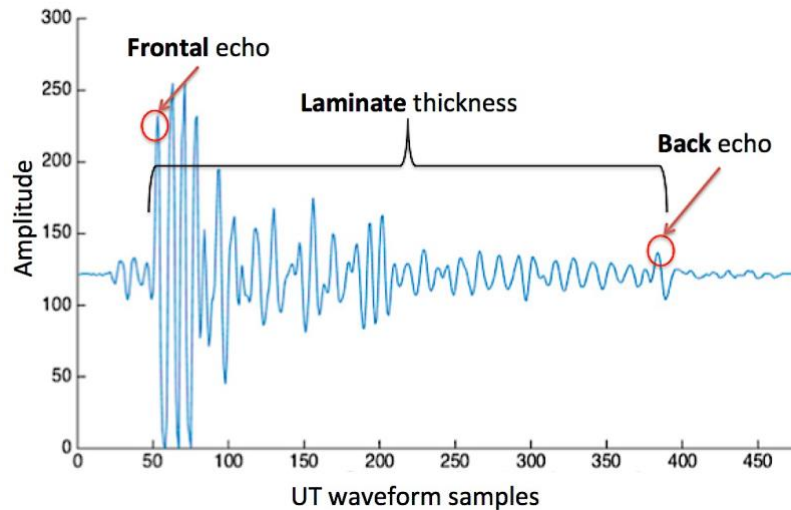


Figure 68. Generic UT waveform of the CFRP drilled laminate with the indication of the total laminate thickness and of the adhesive layer thickness.

4.4.5.4 3D Thickness reconstruction for the Quality Assessment of the drilling process

To perform the quality assessment of the drilling process on the CFRP drilled laminate, that is the verification of Volcano effect (push-out delamination) the calculated thicknesses are presented and analysed. In Figure 69 the cubic interpolation of the total CFRP drilled laminate thickness is reported. By observing the figure the presence of the Volcano effect is clearly evident with a maximum height of 0.74 mm.

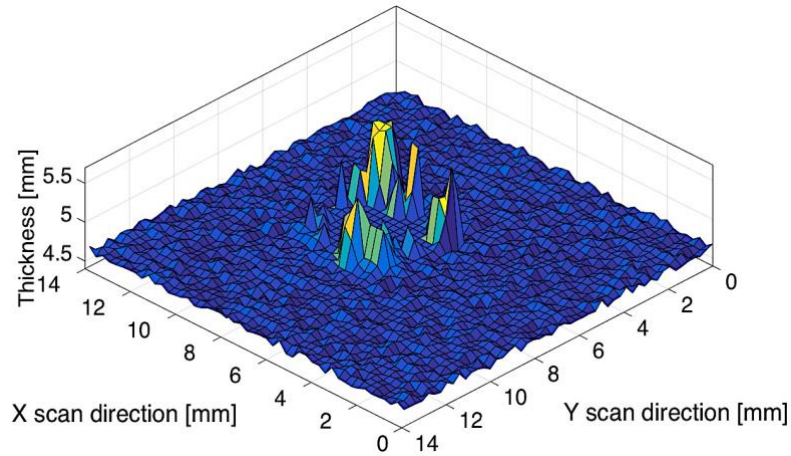


Figure 69. Cubic interpolation of the total CFRP drilled laminate thickness. The presence of Volcano effect is clearly evident.

The coloured map of the drilled CFRP laminate thickness variation is reported in the Figure 70 confirms the presence of the Volcano effect and evidences its orientation at -45° . This because the more exterior fiber layer is proper oriented at -45° . Moreover it can be noticed that the thickness variation (of the drilled area) ranges from ~ 4.78 mm to 5.52 mm.

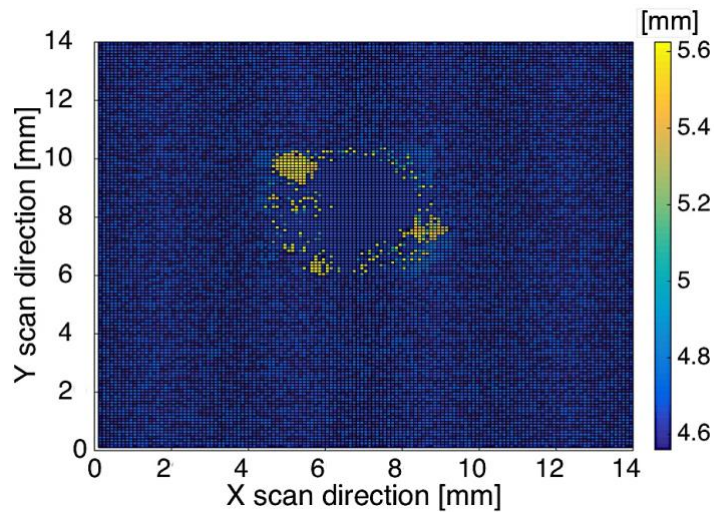


Figure 70. View from above of the total CFRP drilled laminate thickness showing the Volcano effect orientation at -45° and a thickness variation ranging between 4.78 and 5.52 mm.

4.5 Conclusions

An advanced ultrasonic non-destructive evaluation (UT NDE) system based on full volume (FV) ultrasonic scan procedure through pulse-echo immersion testing was utilized for the inspection of three diverse carbon fiber reinforce polymer (CFRP) aeronautical components. The utilized UT NDE system utilized is made of a purposely designed hardware configuration and two custom made software codes developed at the Fraunhofer Joint Laboratory of Excellence on Advanced Production Technology, Naples, Italy.

The first case study under examination concerned the advanced UT non-destructive inspection of 8 CFRP non crimp fabric (NCF) laminates (one not impacted and seven subjected to impact tests with different impact energies) to achieve the following goals:

1. metrological characterization of the not impacted NCF laminate in terms of stacking sequence fiber verification and actual thickness estimation
2. quality assessment of the 7 CFRP NCF in terms of damage development analysis: damage transition in the stacking sequence and damage position in the whole composite material volume.

The results showed that the FV-UT NDE technique is a very efficient tool for the metrological evaluation and damage characterization of impacted NCF composites. The NCF laminate estimated thickness values were very close to the nominal values and the fiber orientations were found consistent with the designed stacking sequence. The impact damage development was effectively characterized by evaluating the damage position in the laminate thickness direction and by identifying the different damage shapes at interfaces between layers with diverse fiber orientations in the stacking sequence.

The second case study regarded the quality assessment of the bonding process of CFRP adhesive bonded joint laminates in terms of adhesive layer homogeneity evaluation and 3D thickness reconstruction of both adhesive layer and entire laminates.

In this case, a not uniform adhesive layer was found. In particular, the presence of a double slope of the adhesive layer was observed. In particular the slope rises along the y scan direction, ranging between -14.5° and -17.8° , and it decreases along the x scan direction, ranging between 5.8° and 12.3° . Finally the thickness of the internal adhesive layer globally varies from 0.968 mm to 0.691 mm.

The third case study concerned the quality assessment of the drilling process of CFRP laminates in terms of drilling process evaluation and push-out delamination characterization through a 3D thickness reconstruction.

The obtained results showed the presence of the Volcano effect and evidencing its orientation at -45° and a thickness variation of the drilled area ranges from about 4.78 mm to 5.52 mm. Moreover, the 3D thickness reconstruction of the drilled CFRP laminate highlighted very clearly the presence of the Volcano effect with a measured maximum height equal to 0.74 mm.

As conclusions, the proposed FV UT scanning procedure together with the developed software codes show a high capability to carry out a thorough CFRP composites characterization in terms of metrological characterization (stacking sequence fiber verification and actual thickness estimation), damage development analysis (damage transition in the stacking sequence and damage position in the composite material volume), quality assessment of process and 3D thickness reconstruction of defects.

4.6 Future step

The advanced UT NDE system and the two custom-made analysis software codes will be utilized to perform the UT inspection on other types of aeronautical components.

The integration between the UT images of the internal structure of the examined samples and their 3D CAD model is already in a development phase. This integration will correspond to spread the UT images on the 3D CAD model of the inspected specimens allowing a complete defects representation (UT images reported on 3D CAD model).

Furthermore, in order to improve the speed of the UT data acquisition the advanced UT NDE scanning system will be equipped with a newest advanced instrumentations (e.g. a new digital oscilloscope with higher sampling frequency) that will require an up-date of the developed software codes.

References

- [1] www.boeing.com
- [2] Segreto T, Caggiano A, Teti R. Quality assurance of brazed copper plates through advanced ultrasonic NDE. *Procedia CIRP* 2016; 55:194-199.
- [3] Teti R. Ultrasonic identification and measurement of defects in composite material laminates. *CIRP Annals* 1990; 39/1: 527-530.
- [4] Caggiano A, Centobelli P, Nele L, Teti R. Multiple Sensor Monitoring in Drilling of CFRP/CFRP Stacks for Cognitive Tool Wear Prediction and Product Quality Assessment. *Procedia CIRP* 2017; 62:3-8.
- [5] Segreto T, Bottillo A, Caggiano A, Teti R, Ricci F. Full-volume ultrasonic technique for 3D thickness reconstruction of CFRP aeronautical components, 2017.
- [6] Graff KF. A history of ultrasonics, in *Physical Acoustics*, XV, Academic Press, New York, 1982.
- [7] Sokolov S, *Phy. Z.* 36 (142), 1935 and *Techn. Physic USSR* 2, 522, 1935.
- [8] Peter J. Shull. *Non destructive evaluation: theory, techniques, and applications*, CRC Press, 2002.
- [9] Firestone FA. Patent n. US 2280226A. Flaw detecting device and measuring instrument, 1942.
- [10] McNulty JF. Patent n. US3260105A. Ultrasonic testing apparatus and method, 1966.
- [11] Teti R. Ultrasonic identification and measurement of defects in composite material laminates. *CIRP Annals* 1990; 39/1: 527-530.
- [12] Casperson R, Knöppchen A, Pohl R, Zimne L, Bode J. Manufacturing of reference defects for NDT using low-energy EDM. *Proceedings of 19th World Conference on Non-Destructive Testing* 2016; 1-10.

- [13] Alobaidi WM, Al-Rizzo HM, Sandgren E. NDT applied to the detection of defects in oil and gas pipes: a simulation-based study. ASME 2015 Int. Mech. Eng. Congr. Expo. 2015; 2B: Advanced Manufacturing.
- [14] Teti R. Machining of Composite materials, CIRP Annals – Manufacturing Technology 2002; 51(2):611-634.
- [15] Wahab MA. Joining composites with adhesives: theory and applications. DEStech Publications, Inc., Lancaster, Pennsylvania, USA; 2016.
- [16] Liganiso LZ, Anandjiwala RD. Fibre-reinforced laminates in aerospace engineering. Advanced composite materials for aerospace engineering 2016; 4:101-127.
- [21] www.airbus.com
- [17] Mallick PK. Fiber-reinforced composites: materials, manufacturing, and design, 3rd ed. CRC Press Taylor & Francis Group; 2007.
- [18] Nayak NV. Composite materials in aerospace applications. International Journal of Scientific and Research Publications 2014; 4(9):1-10.
- [19] Mangalgi PD. Composite materials for aerospace applications. Bulletin of Materials Science 1999; 22:657-664.
- [20] Witik RA, Gailleb F, Teuscher R, Ringwald H, Michaud V. Economic and environmental assessment of alternative production methods for composite aircraft components. J Cleaner Production 2012; 29-30: 91-102
- [23] Hsu DK. Non-destructive evaluation (NDE) of aerospace composites: ultrasonic techniques. NDE of polymer matrix composites 2013, 397-422 pulse
- [24] https://www.faa.gov/regulations_policies/
- [22] Segreto T, Bottillo A, Teti R. Advanced ultrasonic non-destructive evaluation for metrological analysis and quality assessment of impact damaged non-crimp fabric composites, 2015.
- [25] Scott IG, Scala CM. A review of non-destructive testing of composite materials, NDT International 1982; 15(2):75-86.

- [26] Gholizadeh S. A review of non-destructive testing methods of composite materials. *Procedia Structural Integrity* 2016; 1:50-57.
- [27] Blitz J, Simpson G. *Ultrasonic methods of non-destructive testing*. Springer; 1995.
- [28] *Metals Handbook, Ninth Edition, Volume 17, Non-destructive Evaluation and Quality Control*, 1989, ASM International Handbook Committee, ASM International, Metals Park, OH, USA.
- [29] Lu Z, Yang C, Qin D, Luo Y, Momayez M. Estimating ultrasonic time-of-flight through echo signal envelope and modified Gauss Newton method. *Measurement* 94 (2016) 355–363.
- [30] Kessels JFA, Jonker AS, Akkerman R. Optimising the flow pipe arrangement for resin infusion under flexible tooling. *Composites Part A: Applied Science and Manufacturing* 2007; 38: 2076-2085.
- [31] <http://www.jleapt-unina.fraunhofer.it/>
- [32] USIP 12 Operating instruction. Krautkrämer-Branson
- [33] The LeCroy MODEL 9400 DIGITAL OSCILLOSCOPE OPERATORS MANUAL
- [34] Stäubli RX60L robot - CS7B controller Operator's Manual
- [35] Stäubli CS7B controller Operator's Manual
- [36] Poorzeinolabedin M, Parnas L, Dashatan S.H. Resin infusion under flexible tooling process and structural design optimization of the complex part. *Material and Design* 2014; 64: 450-455
- [37] Adden S, Horst P. Damage propagation in non-crimp fabrics under bi-axial static and fatigue loading. *Comp Sci & Technol* 2006; 66: 626-633.
- [38] Williams C, Summerscalest J, Grove S. Resin Infusion under Flexible Tooling (RIFT): a review. *Composites Part A* 1996, 27A:517-524
- [39] Abrate S. *Impact on composite structures*, Cambridge Univ. Press; 1998
- [40] Higgins A. Adhesive bonding of aircraft structures. *International Journal of Adhesion & Adhesives* 2000; 20:367-376.

- [41] Da Silva LFM, Öchsner A, Adams RD. Handbook of Adhesion Technology, Springer-Verlag Berlin Heidelberg, 2011.
- [42] Tamborrino R., Palumbo D, Galietti U, Aversa P, Chiozzi S, Luprano VAM. Assessment of the effect of defects on mechanical properties of adhesive bonded joints by using non destructive methods. *Composites Part B: Engineering* 2016; 91:337-345.
- [43] ASTM D3165 - 07(2017) - Standard Test Method for Strength Properties of Adhesives in Shear by Tension Loading of Single-Lap-Joint Laminated Assemblies
- [44] ASTM D2093 - 03(2017) - Standard Practice for Preparation of Surfaces of Plastics Prior to Adhesive Bonding.
- [45] Sanjat K. Mazumdar, *Composites Manufacturing – Materials, Product, and Process Engineering*. CRC Press LLC 2002; 6: 1-135
- [46] Lopresto V, Caggiano A, Teti R. High Performance Cutting of Fibre Reinforced Plastic Composite Materials. *Procedia CIRP* 2016; 46:71-82.
- [47] Caggiano A, Angelone R, Teti R. Image Analysis for CFRP Drilled Hole Quality Assessment. *Procedia CIRP* 2017; 62:440-445.
- [48] Dharan CKH, Won MS. Machining parameters for an intelligent machining system for composite laminates. *Int. J. Machine Tools Manuf.* 2000; 40(3):415-426.
- [49] Thagard JR, Okoli OI, Liang Z, Wang HP, Zhang C. Resin infusion between double flexible tooling: prototype development. *Composites Part A: Applied Science and Manufacturing* 2003, 34/9: 803-811.